



Contents lists available at ScienceDirect

Saudi Pharmaceutical Journal

journal homepage: www.sciencedirect.com



Original article

## Synthesis, biological evaluations and molecular modelling studies of novel indolin-2-ones designing as FGFR inhibitors

Güneş Çoban<sup>a,\*</sup>, Fadime Aydın Köse<sup>b</sup><sup>a</sup>Department of Pharmaceutical Chemistry, Faculty of Pharmacy, Ege University, 35040 Bornova, Izmir, Turkey<sup>b</sup>Department of Biochemistry, Faculty of Pharmacy, Ege University, 35040 Bornova, Izmir, Turkey

## ARTICLE INFO

## Article history:

Received 18 April 2019

Accepted 10 July 2019

Available online 11 July 2019

## Keywords:

FGF receptors

Indolin-2-one

Molecular modelling

Enzyme inhibition

Cell culture

## ABSTRACT

A series of novel 3,5-disubstituted indolin-2-ones were designed and synthesized as selective FGFR inhibitors. In the design process of 3,5-disubstituted indolin-2-ones for FGFRs, molecular docking studies were performed to generate and optimize novel compounds which have FGFR inhibitory potency, theoretically. *In vitro* enzyme inhibitory and selectivity profiles of the synthesized compounds, and their cytotoxicity against NIH-3T3 cells were evaluated. According to enzyme inhibition assay, compound **A1** (FGFR1-4; IC<sub>50</sub> = 19.82; 5.95; 1419; 37150 nM), compound **A5** (FGFR1-4; IC<sub>50</sub> = 1890; Nd; 6.50; 18590 nM) and compound **A13** (FGFR1-4; IC<sub>50</sub> = 6.99; 1022; 17090; 8993 nM) have displayed best inhibitory potency against FGFR2, FGFR3 and FGFR1, respectively. The studied compounds have displayed low affinity to FGFR4 in comparison with other isoforms. Molecular docking study data were used to determine the binding orientations of the synthesized compounds inside FGFRs in accordance with enzyme inhibition assay data. Molecular dynamics simulations and free energy calculations were performed to determine stability, binding modes and dynamics behaviors of compound **A1**, **A5** and **A13** inside FGFR-2, FGFR-3 and FGFR-1, respectively. The compounds bearing aromatic groups at the C5 position of indolin-2-one could be lead compounds for the development of more effective and selective FGFR1-3 inhibitors.

© 2019 Production and hosting by Elsevier B.V. on behalf of King Saud University. This is an open access article under the CC BY-NC-ND license (<http://creativecommons.org/licenses/by-nc-nd/4.0/>).

## 1. Introduction

The fibroblast growth factor receptors (FGFRs) are subtype of tyrosine kinases (RTKs), which are responsible for cell morphogenesis, proliferation, differentiation and migration in embryogenesis, and contribute organogenesis, angiogenesis and development of skeleton in adult organism as mitogen (Ahmad et al., 2012). The FGFRs are encoded by four receptor genes namely FGFR1-4, and they share similar homology as 75–92% at tyrosine kinase domain in human (Ahmad et al., 2012; Li et al., 2017). It is reported that the closest homology seems between FGFR1 and FGFR2, while furthest homology seems between FGFR1 and FGFR4. Each FGFR monomers protein consist of an extracellular ligand-binding region, a single-

pass transmembrane domain and an intracellular tyrosine kinase domain. Activators binding to FGFRs trigger receptor dimerization, afterward, initiate the cascade of downstream signaling pathways such as Ras-Raf-MapK, PI3K-Akt, STATs and PLC $\gamma$  to regulate crucial physiological processes (Heinzle et al., 2011; Wang et al., 2018). The abnormal signaling related to FGFR cascade was associated with several cancers such as urothelial, breast, endometrial, liver, gastric systems, bladder and multiple myeloma. Furthermore, various alterations in FGFRs have been identified as oncogenic drivers in the development and progression of human tumors.

In previous studies, FGFR1 gene amplification and mutation are detected in lung adenocarcinoma, breast cancer, urothelial carcinoma and oral squamous cell carcinomas (Kim et al., 2018). FGFR2 gene amplification and/or mutation are shown in stomach, lung, breast, and ovarian cancers, bladder cancer, invasive lobular carcinoma and multiple myeloma (Kas et al., 2018). FGFR3 amplification has been observed in bladder cancer, also it has been suggested that these mutations contribute to the development of cervical and bladder cancers, multiple myeloma, spermatocytic seminoma and seborrhic keratosis. Besides, K535/E550 mutations of FGFR4 are associated with rhabdomyosarcoma (Heinzle et al., 2011; Liang et al., 2013; Turner and Grose, 2010).

\* Corresponding author.

E-mail address: [gunes.coban@ege.edu.tr](mailto:gunes.coban@ege.edu.tr) (G. Çoban).

Peer review under responsibility of King Saud University.



Production and hosting by Elsevier

According to reported scientific articles about FGFRs, highly conserved ATP binding site is divided into five subregions: hydrophobic regions I and II, adenine, ribose and phosphate-binding regions (Wang et al., 2018). Hydrophobic region I is a vast hydrophobic pocket that is formed by several hydrophobic amino acid residues. This region is also a selective pocket that forms van der Waals interactions with hydrophobic groups which enter the pocket. Besides of van der Waals interactions, some amino acid residues of hydrophobic region I form crucial H bonds with the groups that enter the region. Hydrophobic region II is another hydrophobic area that is located outside ATP binding site, plays an important role in binding small molecule inhibitors by interacting with lipophilic moieties. The adenine region or hinge region is major binding site in which heterocyclic templates that mimic binding mode of adenine in the ATP form several H bonds with amino acid residues. The nucleotide domain is located adjacent to hydrophobic region II and rarely used in binding inhibitors. The hydroxyl in the ribose ring of ATP forms a hydrogen bond with amino acid residue as Asp568 in FGFR1. A few numbers of inhibitors such as GSK1070916 (1), NP603 (2) and SU5402 (3) have been reported to form H bond with Asn568 (FGFR1 residue numbering) in the nucleotide domain (Fig. 1) (Liang et al., 2013). The phosphate region is located domain of phosphates in the ATP in FGFRs, that has reported forming a H bond with a small molecule (Erdafitinib (4)) which may considerably contribute to overall binding affinity and specificity (Fig. 1) (Wang et al., 2018).

There are several FGFRs inhibitors approved by United States Food and Drug Administration and European Medicines Agency for treatment of FGFRs related cancers such as idiopathic

pulmonary fibrosis (nintedanib (5)); renal cell carcinoma and soft tissue sarcomas (pazopanib (6)); Philadelphia chromosome-positive chronic myeloid leukemia or acute lymphoblastic leukemia (ponatinib (7)); colorectal cancer and gastrointestinal stromal tumor (regorafenib (8)); differentiated thyroid cancer (lenvatinib (9)); and evaluated in clinical trials at different stages such as AZD-4547 (10) in phase III, BGJ-398 (11) in phase II, and LY-2874455 (12) in phase II (Fig. 1) (Wang et al., 2018; Porta et al., 2017). Nevertheless, currently approved FGFR inhibitors are multi-target inhibitors such as nintedanib (5), pazopanib (6), ponatinib (7), regorafenib (8), and lenvatinib (9) which display implementing antitumor efficiency primarily through targeting other RTKs rather than FGFRs (Zhu et al., 2017; Ghedini et al., 2018; Wei et al., 2018). Therefore, developing more selective inhibitors are needed to tumor suppression by directly targeting FGFRs. Due to this necessity, there are some FGFR inhibitors evaluated in clinical trials have been developed as more selective to FGFRs (Ghedini et al., 2018). The outputs of these investigations will give some opportunities to validate more potent and selective FGFR inhibitors for single anticancer therapies.

SU4984 (13) and SU5402 (3) are the well-known FGFR inhibitor and are based on an oxindole core (indolin-2-ones) (Fig. 1). They inhibit kinase activity of FGFR1 and showed differential specificity toward other RTKs. Crystal structures of tyrosine kinase domain of FGFR1 in complex with SU4984 (13) and SU5402 (3) were reported by Mohammadi and coworkers (Mohammadi et al., 1997). In title study, it was detected that oxindole of SU4984 (13) occupied the adenine region and extended to contact residues as Glu562 and Ala564 in the hinge region between two kinase lobes of FGFR1.

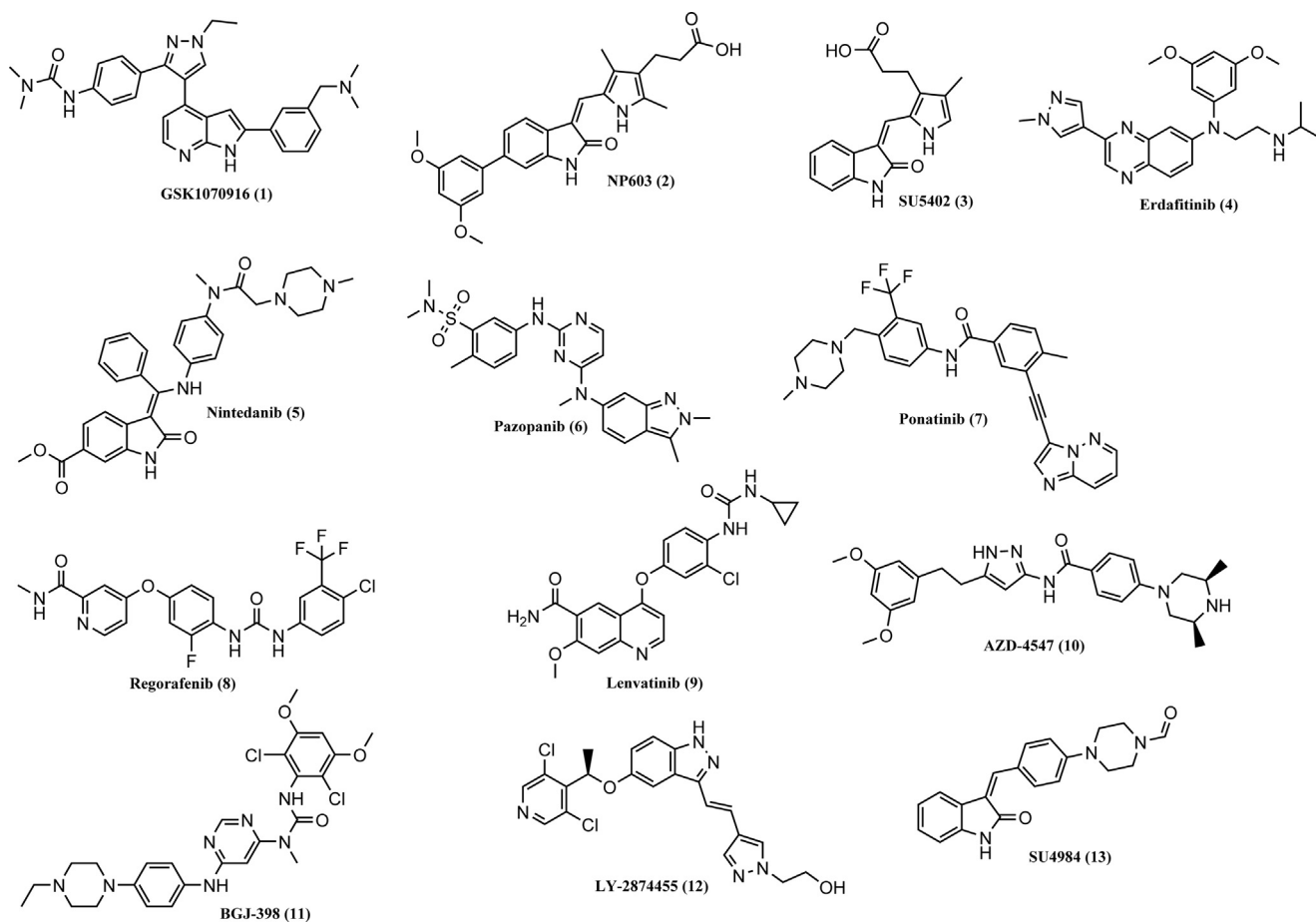


Fig. 1. Chemical structures of some representative FGFR inhibitors.

In addition, it was found that phenyl ring of SU4984 (13) made an oxygen-aromatic contact with carbonyl oxygen of Ala564 and piperazine ring of SU4984 (13) constituted van der Waals contact with Gly567 in FGFR1 (Mohammadi et al., 1997). Besides, it was determined that oxindole of SU5402 (3) occupied the adenine region as similar as oxindole of SU4984 (13), but the orientations of the bicyclic ring systems differ by opposite. It was reported that an intramolecular hydrogen bond was formed by nitrogen of the pyrrole ring and oxygen of the oxindole, and the methyl group of the pyrrole ring formed a van der Waals contact with Gly567 and the carboxy ethyl group at the 3 position of the pyrrole ring formed a hydrogen bond with the side chain of Asp568 (Mohammadi et al., 1997). In addition, the well-known multi-targeted RTK inhibitor as nintedanib (5) and other FGFR inhibitor as NP603 (2) contain an oxindole core (Fig. 1). There are many studies were focused on oxindoles for the development of RTK inhibitors have been reported. In a study was reported by Sun and coworkers, 3-(4-substituted benzylidene)indolin-2-ones bearing several cyclic and acyclic amines at the 4 positions of benzylidene group were developed to evaluate the inhibition of cellular tyrosine activity (Sun et al., 1998). Another study reported by Chen and coworkers mentioned that some oxindole-based RTK inhibitors were developed which contain 4-substituted benzylidene groups at the 3 positions of indolin-2-on inhibiting c-Kit kinase (Chen et al., 2014). Lastly, Li and coworkers have reported to synthesis some kinase inhibitors bearing several cyclic amines at the 4 positions of benzylidene group substituted on 3 positions of the indolin-2-one core and bearing phenyl or pyridyl substituted thiazole ring at 3 positions of the indolin-2-one core, and these showed inhibitory potency against cancer stem cells (Li et al., 2014).

We envisioned that development of new FGFR inhibitors based on SU4984 (13) using two main approaches for design. The first approach for improving inhibitory activity on FGFRs is the addition of several aromatic rings at the 5 position of oxindole core of SU4984 (13) aiming to occupy hydrophobic region I (Fig. 2). Considered second approach is as to change and remove the terminal formyl group of piperazine and changing of piperazine ring with several six-membered rings such as morpholine and 4-hydroxypiperidine (Fig. 2). Herein, we describe the design and synthesis 5-substituted-3-(4-substitutedbenzylidene)indolin-2-one derivatives, and report inhibitory potencies on FGFRs, cytotoxic

profile against NIH-3T3 cells and docking study of these derivatives and molecular dynamics simulation study of compound **A1**, **A5** and **A13**.

## 2. Experimental

### 2.1. Chemistry

#### 2.1.1. Materials and methods

Melting points were detected with capillary melting point apparatus (Stuart SMP30, Staffordshire, UK). The IR spectra of the compounds were monitored by attenuated total reflectance (ATR) (PerkinElmer Spectrum 100 FT-IR, Shelton, USA). The nuclear magnetic resonance (NMR) spectra (400 MHz for  $^1\text{H}$  NMR and 100 MHz for  $^{13}\text{C}$  NMR) were recorded in the deuterated solvent on AS400 Mercury Plus NMR Varian (Varian Inc., Palo Alto, CA, USA). Chemical shifts were measured in parts per million ( $\delta$ ). Coupling constants ( $J$ ) are reported in hertz (Hz). LC/MS was recorded on a Thermo MSQ Plus (San Jose, CA, USA) mass spectrometer using ESI (+) method. Elemental analyses were carried out by Leco TruSpec Micro CHNS (Leco, St. Joseph, MI, USA) and were within  $\pm 0.4\%$  of the theoretical values. Analytical thin-layer chromatography (TLC) was exerted on Merck silica gel plates (Kieselgel 60 F<sub>254</sub>) with detection by UV light (254 nm); column chromatography was carried out using Merck silica gel 60 (63–200 mm diameter). All starting materials and reagents were high-grade commercial products.

#### 2.1.2. Synthesis of 5-bromoindolin-2-one

5-Bromoisatin (11.5 g, 5.1 mmol) was heated in 30 ml of hydrazine hydrate to 140–160 °C for 4 h. The mixture was cooled to room temperature and then acidified to pH 2 with 6 N hydrochloric acid. The acidified mixture was left at room temperature during two days then formed precipitate was collected by vacuum filtration, washed with water and dried at room temperature. 5-Bromoindolin-2-one was obtained 5.61 g (52% yield).

#### 2.1.3. Synthesis of 4-substituted benzaldehydes

23 mmol of an appropriate amine (morpholine, 4-hydroxypiperidol, 4-methylpiperazine and piperazine) was solved in 20 ml of dry DMF. Anhydrous potassium carbonate (3.17 g,

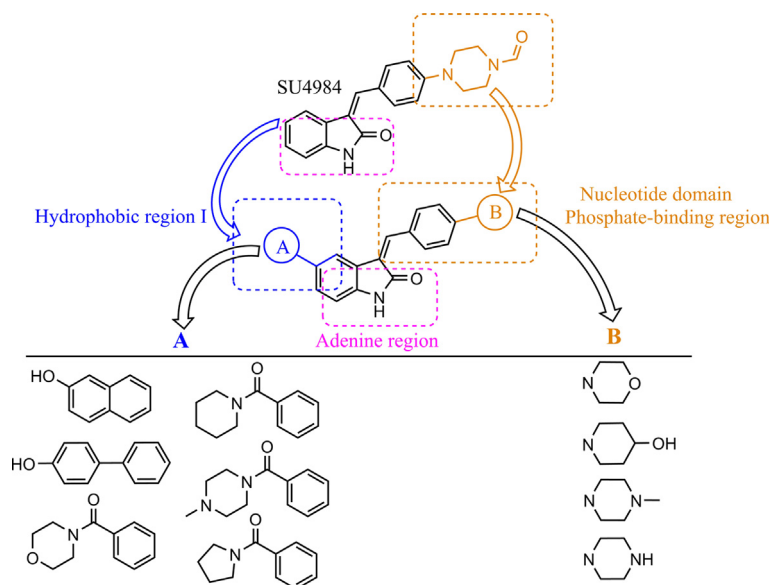


Fig. 2. Design of new FGFR inhibitors.

23 mmol) was added to mixture and the mixture was stirred for 15 min. Then, *p*-fluorobenzaldehyde (1 g, 7.6 mmol) was added and the mixture was stirred at 80 °C for 10 h. The mixture was cooled to room temperature, filtered and DMF was concentrated in vacuo. The 30 ml of water was added to residue and aqueous layer was extracted with 2 × 20 ml of chloroform. The organic layer was dried with anhydrous sodium sulfate and concentrated in vacuo. The resultant residue was then purified by column chromatography (Dichloromethane/methanol:10/1).

#### 2.1.4. Synthesis of 4-(4-formylphenyl)piperazine-1-carbaldehyde

Piperazine (1.98 g, 23 mmol) was solved in 20 ml of dry DMF. Anhydrous potassium carbonate (3.17 g, 23 mmol) and sodium iodide (3.45 g, 23 mmol) were added to mixture and the mixture was stirred for 15 min. Then, *p*-fluorobenzaldehyde (1 g, 7.6 mmol) was added and the mixture was stirred at 130 °C for 4 h. The mixture was cooled to room temperature, filtered and DMF was concentrated in vacuo. The 30 ml of water was added to residue and aqueous layer was extracted with 2 × 20 ml of chloroform. The organic layer was dried with anhydrous sodium sulfate and concentrated in vacuo. The resultant residue was then purified by column chromatography (Dichloromethane/methanol:10/1).

#### 2.1.5. Synthesis of 5-bromo-3-(4-substituted benzylidene)indolin-2-ones

A reaction mixture of 3.14 mmol (0.625 g) of 5-bromoindolin-2-one, 3.14 mmol of 4-substituted benzaldehydes and 0.5 ml piperidine in 50 ml of ethanol was stirred at 90 °C for 5 h. After cooling, the precipitate was filtered, washed with cold ethanol, and dried. The compounds were obtained as yellow-orange solids.

#### 2.1.6. Synthesis of 4-bromobenzamide derivatives

4-Bromobenzoyl chloride (1 g, 4.56 mmol) was added into 15 ml of THF and the mixture was cooled to 0 °C. A solution of 4.78 mmol of an appropriate amine (morpholine, piperidine, 4-methylpiperazine and pyrrolidine) and 0.7 ml of TEA in THF (25 ml) were added dropwise, and the mixture was stirred at 0 °C for 3 h. Water was added to mixture and the products were extracted with ethyl acetate (x2). The combined organic extracts were washed with brine, dried over anhydrous sodium sulfate and concentrated in vacuo to give an appropriate 4-bromobenzamide as gum.

#### 2.1.7. Synthesis of 6-hydroxynaphthylboronic acid pinacol ester

A mixture of 6-bromonaphthalen-2-ol (0.45 g, 2 mmol), bis(pinacolato)diboron (0.76 g, 3 mmol), potassium acetate (0.59 g, 6 mmol) and [1,1'-bis(diphenylphosphino)ferrocene]dichloropalladium(II) complex with dichloromethane (0.075 g, 0.09 mmol) were stirred in 15 ml of 1,4-dioxane at 100 °C for 45 min in microwave reactor. After cooling to room temperature, the mixture was concentrated in vacuo. Then the resultant residue was purified by column chromatography (n-Hexane/ethyl acetate:6/1).

#### 2.1.8. Synthesis of 4'-hydroxy-[1,1'-biphenyl]boronic acid pinacol ester

A mixture of 4'-bromo-[1,1'-biphenyl]-4-ol (0.5 g, 2 mmol), bis(pinacolato)diboron (0.76 g, 3 mmol), potassium acetate (0.59 g, 6 mmol) and [1,1'-bis(diphenylphosphino)ferrocene]dichloropalladium(II) complex with dichloromethane (0.075 g, 0.09 mmol) were stirred in 15 ml of 1,4-dioxane at 100 °C for 45 min in microwave reactor. After cooling to room temperature, the mixture was concentrated in vacuo. The resultant residue was then purified by column chromatography (n-Hexane/ethyl acetate:6/1).

#### 2.1.9. Synthesis of 4-substituted amidophenylboronic acid pinacol esters

A mixture of an appropriate 4-bromo-*N*-substituted benzamide (2 mmol), bis(pinacolato)diboron (0.76 g, 3 mmol), potassium acetate (0.59 g, 6 mmol) and [1,1'-bis(diphenylphosphino)ferrocene]dichloropalladium(II) complex with dichloromethane (0.075 g, 0.09 mmol) were stirred in 15 ml of 1,4-dioxane at 100 °C for 45 min in microwave reactor. After cooling to room temperature, the mixture was concentrated in vacuo. The resultant residue was then purified by column chromatography (Dichloromethane/methanol:15/1).

#### 2.1.10. Synthesis of 5-(6-hydroxynaphthalen-2-yl)-3-(4-substituted benzylidene)indolin-2-ones

6-Hydroxynaphthylboronic acid pinacol ester (1.5 mmol) and (*E,Z*)-5-bromo-3-(4-substituted benzylidene)indolin-2-one (1 mmol) were added in 10 ml of 1,4-dioxane. Then, tetrakis(triphenylphosphine)palladium (0.046 g, 0.04 mmol) and 2 ml of 2 M potassium carbonate were added this mixture. The mixture was stirred at 120 °C for 30 min in microwave reactor. After cooling to room temperature, the mixture was concentrated in vacuo. The resultant residue was washed with water, dried and purified by column chromatography (Dichloromethane/methanol:25/1 then Dichloromethane/methanol:10/1).

#### 2.1.11. Synthesis of 5-(4'-hydroxy-[1,1'-biphenyl]-4-yl)-3-(4-substituted benzylidene)indolin-2-ones

4-Hydroxy-[1,1'-biphenyl]boronic acid pinacol ester (1.5 mmol) and (*E,Z*)-5-bromo-3-(4-substituted benzylidene)indolin-2-one (1 mmol) were added in 10 ml of 1,4-dioxane. Then, tetrakis(triphenylphosphine)palladium (0.046 g, 0.04 mmol) and 2 ml of 2 M potassium carbonate were added this mixture. The mixture was stirred at 120 °C for 30 min in microwave reactor. After cooling to room temperature, the mixture was concentrated in vacuo. The resultant residue was washed with water, dried and purified by column chromatography (Dichloromethane/methanol:25/1 then Dichloromethane/methanol:10/1).

#### 2.1.12. Synthesis of 5-(4-substituted amidophenyl)-3-(4-substituted benzylidene)indolin-2-ones

An appropriate 4-substituted amidophenylboronic acid pinacol esters (1.5 mmol) and (*E,Z*)-5-bromo-3-(4-substituted benzylidene)indolin-2-one (1 mmol) were added in 10 ml of 1,4-dioxane. Then, tetrakis(triphenylphosphine)palladium (0.046 g, 0.04 mmol) and 2 ml of 2 M potassium carbonate were added this mixture. The mixture was stirred at 120 °C for 30 min in microwave reactor. After cooling to room temperature, the mixture was concentrated in vacuo. The resultant residue was washed with water, dried and purified by column chromatography (Dichloromethane/methanol:25/1 then Dichloromethane/methanol:10/1).

The intermedia compounds which have the Chemical Abstracts Service (CAS) number was given with their CAS numbers in Table S1 in [Supplementary materials](#).

## 2.2. Molecular modelling study

### 2.2.1. Homology modelling

Sequence of human FGFR3 (P22607) was taken from The Universal Protein Resource Knowledgebase (UniProtKB). Homology model of FGFR3 was built using MODELLER module of USCF Chimera software ([Webb and Sali, 2014](#)). The crystal structure of FGFR2 (PDB id: 3B2T resolved at 1.8 Å) obtained from the RCSB Protein Data Bank has been selected as template structure to construct homology model. The selected PDB file displays a primary amino acid sequence identity of 88.52% with FGFR3. Following



the construction of model, crude model was aligned with chain A of crystal structure of FGFR2 (PDB id: 3B2T) for indicating binding site residues of the model. The crude model was parametrized with AMBER99SB force field, solvated in an octahedral box with TIP3P water molecules with 10 Å distance between protein surface and box boundary and neutralized with appropriate number of sodium counter ions (Hornak et al., 2006; Jorgensen et al., 1983). The preparation of the model for energy minimization was practiced using xleap module of AmberTools 16. The model was exposed to an energy minimization with Sander.MPI module of AmberTools 16 (Case et al., 2012).

### 2.2.2. Ligand docking

The chemical structures of indolin-2-ones were generated with builder panel of MOE2016.08 and protonated using the protonate 3D protocol. The protonated structures were exposed to an energy minimization with MOE.2016.08 using MMFF94x force field (Molecular Operating Environment, 2016; Halgren, 1996). The crystal structures of FGFR1 (PDB id: 5B7V resolved at 2.15 Å), FGFR2 (PDB id: 3RI1 resolved at 2.1 Å) and FGFR4 (PDB id: 4QRC resolved at 1.9 Å) were taken from the RCSB Protein Data Bank (<http://www.rcsb.org/pdb>). For FGFR1 chain B was kept for docking study, and chain A, heteroatoms, water molecules were deleted from the pdb file. For FGFR2 and FGFR4, chain A was kept for docking study and chain B, heteroatoms, water molecules were deleted from the pdb file. The proteins were parametrized with AMBER99SB force field, solvated in an octahedral box with TIP3P water molecules with 10 Å distance between protein surface and box boundary and neutralized with appropriate number of sodium counter ions (Hornak et al., 2006; Jorgensen et al., 1983). The preparation of the proteins for energy minimization was practiced using xleap module of AmberTools 16. The proteins were exposed to an energy minimization with Sander.MPI module of AmberTools 16 (Case et al., 2012).

FGFR1, FGFR2, FGFR4 and homology model of FGFR3 were prepared for docking study removing water molecules (excluded

water molecules existed in the binding site) and sodium counter ions. The docking study of ligands was performed using GOLD 5.2.1 program with default generic algorithm parameters (Jones et al., 1995, 1997). The studied compounds were docked within a radius of 15 Å around carbon atom of carboxylate group of Asp641 of FGFR1, of Asp644 of FGFR2 and of Asp635 of FGFR3, and carbon atom of guanidine group of Arg616 of FGFR4. Hundred conformations were generated per structure. GoldScore fitness function was used as scoring functions (Jones et al., 1995, 1997). Fig. 3, Figs. S1–S4, Fig. S6 and figures in Tables S2–S5 were created with MOE2016.08 program.

### 2.2.3. Molecular dynamics simulations

Molecular dynamics simulations were performed to apo form of proteins (FGFR1, FGFR2 and FGFR3) and protein-ligand complexes using AMBER12 (Case et al., 2012). The starting protein-ligand complexes were prepared using the suggested docking poses of compound **A1** in FGFR2, of compound **A5** in FGFR3 and of compound **A13** in FGFR1 obtained from docking studies. The partial atomic charges of compounds **A1**, **A5** and **A13** were calculated with AM1-BCC charge model using antechamber module of AmberTools 16 (Case et al., 2012; Jakalian et al., 2000). The apo form of proteins and protein-ligand complexes were prepared for energy minimizations and MD simulations using xleap module of AmberTools 16 (Case et al., 2012). General AMBER force field (gaff) for ligand and AMBER ff99SB force field for proteins were used to become parameterization of the complex systems (Hornak et al., 2006; Wang et al., 2004). The apo forms of FGFR1, FGFR2 and FGFR3, and their complexes with related ligands were neutralized with appropriate number of sodium counter ions. All systems were solvated in an octahedral box with TIP3P water molecules with 10 Å distance between protein surface and box boundary (Jorgensen et al., 1983). Sander.MPI module of AmberTools 16 and pmemd.cuda module of AMBER12 were used to practice energy minimizations and MD simulations of the systems, respectively (Case et al., 2012). To avoid bad steric contacts, the starting systems were

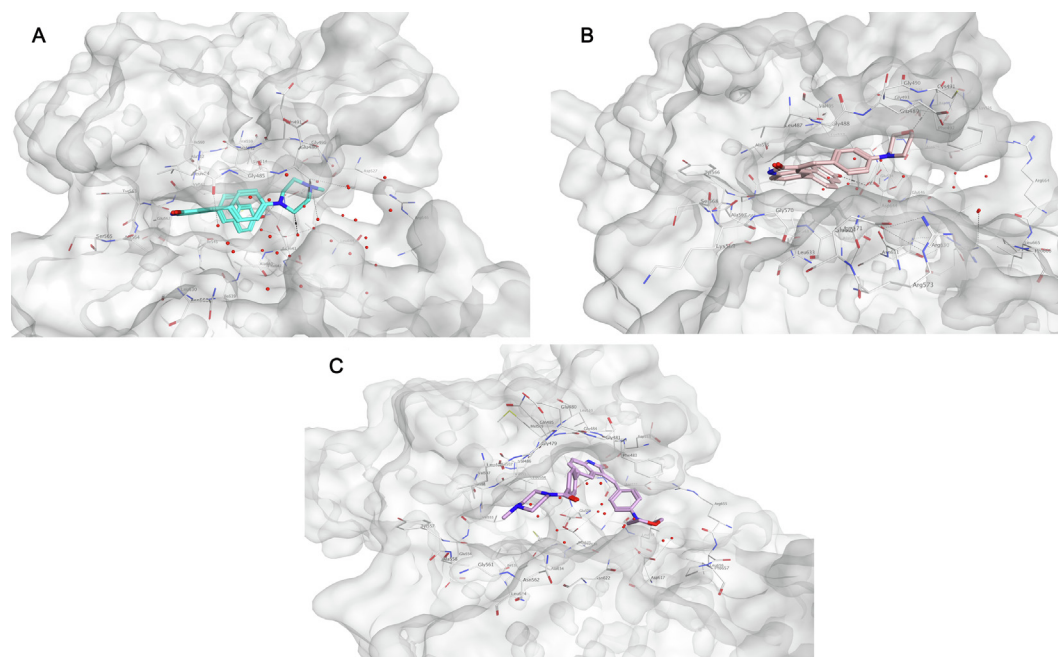


**Fig. 3.** (A) The suggested docking pose of compound **A13** in FGFR1. (B) The suggested docking pose of compound **A1** in FGFR2. (C) The suggested docking pose of compound **A5** in FGFR3. Cyan, pink, light magenta and light grey sticks represent compound **A13**, compound **A1**, compound **A5** and active site residues of FGFR1–3, respectively. The active site residues are named using three letters code. For a clear image, all hydrogen atoms were ghosted. H bonds are represented black dashed lines, respectively. Molecular surfaces of FGFR1–3 were added.

subjected to energy minimization in two steps. In the first step, energy minimizations were performed to restrained initial structures using steepest descent algorithm at 1000 iterations and conjugate gradient methods at 1000 iterations. Following the first step, energy minimization was carried out all systems using steepest descent algorithm at 2500 iterations and using conjugate gradient methods at 2500 iterations. The MD simulations for the systems were practiced at the three steps as heating (0.1 ns), equilibration (2 ns) and production (100 ns). Firstly, the systems were heated from 0 to 300 K with 10 kcal/mol/Å restraint force permitting water molecules and ions to move freely. Secondly, temperature was equilibrated at 300 K using Langevin dynamics with collision frequency of  $1.0 \text{ ps}^{-1}$  in constant volume periodic boundary for the entire systems. The pressure was equilibrated at 1 bar with keeping positional restrains for solute using constant pressure periodic boundary conditions with isotropic position scaling method at 300 K. Lastly, positional constrains were gradually removed keeping temperature at 300 K and pressure at 1 bar. In the equilibration and production steps, the SHAKE algorithm was performed to constrain bond vibrations involving hydrogen atoms (Ryckaert et al., 1997). The Particle Mesh Ewald (PME) method was practiced for long-range electrostatic interactions (Essmann et al., 1995). The time step for all MD simulations has been 2 fs and non-bonded interactions were truncated using cutoff of 10 Å. All systems were subjected to production step for 100 ns. Xmgrace program was used for visualization of trajectories (Grace Development Team). The hydrogen bonding was detected with Cpptraj module of AmberTools 16 using default parameters (Roe and Cheatham III, 2013). The calculations of free binding energies of compounds and energy decomposition analysis were executed with MMPBSA.py.MPI module of AmberTools16 using the Generalized-Born (GB) model from 100 spaced snapshots of unrestrained MD simulations (Miller III et al., 2012). MD snapshots were extracted from free MD simulations using UCSF Chimera package (Pettersen et al., 2004). Figures associated with MD snapshots in supplementary materials section were set-up with MOE2016.08 program.

### 2.3. Biological activity study

#### 2.3.1. Kinase assay

Kinase enzyme inhibition assays were performed by Z'-LYTE assay kit (Z-Lyte- Tyr 4 peptide assay kit, catalog no. PV3193) using FGFR1 (catalog no. PV3146), FGFR2 (catalog no. PV3368), FGFR3 (catalog no. PV3145) and FGFR4 (catalog no. PV3054) supplied from Thermo Fischer Scientific.

Compounds were tested in a doseresponse curve following the kit protocols. Briefly, 10 µL reactions were set up in order to contain 2.5 µL 4X test compounds, 5 µL 2X peptide/kinase mixture and 2.5 µL 4X ATP solution in 384-well plates. The optimal kinases and ATP concentrations for each FGFR were determined by optimization experiments. The kinase concentration was 2 ng/10 µL in FGFR-1 and FGFR-2 assay, 10 ng/10 µL in FGFR-3 and 80 ng/10 µL in FGFR-4 assay. The ATP concentrations were 4 µM in the assay of FGFR-1 and FGFR-2, 10 µM in FGFR-3 assay and 300 µM in FGFR-4 assay. After 1 h of incubation at room temperature, 5 µL of development reagent solution was added to per well, and followed by incubation at room temperature for additional 60 min. The reaction was then stopped by 5 µL of stop solution addition, and the fluorescent signal ratio of 445 nm (coumarin)/520 nm (fluorescein) was determined on a plate reader (VarioSkan Multimode, Thermo Scientific), which reflects the peptide substrate cleavage status and/or the kinase inhibitory activity in the reaction (Jia et al., 2008). Staurosporine was used as a positive control for FGFR inhibition.

The IC50 values of compounds were calculated by nonlinear regression (curve fit) of log concentration versus percent phosphorylation calculated from the emission ratio of 445/520 in Prism GraphPad 5.0 statistical software (San Diego, CA) and values were represented as means ± S.E.M. from three independent experiments.

#### 2.3.2. Cell culture and cytotoxicity assay

The cytotoxic potential of compounds was determined by colorimetric WST-1 (4-[3-(4-Iodophenyl)-2-(4-nitro-phenyl)-2H-5-tetrazolol]-1,3-benzene disulfonate) assay (Roche).

The NIH-3T3 (mouse embryonic fibroblast) cell line was purchased from American Type Culture Collection (ATCC) and cultured at 37 °C in a humidified atmosphere of 5% CO<sub>2</sub> in Dulbecco's modified Eagle's medium (DMEM) supplemented with 10% fetal bovine serum.

For cytotoxicity assay, cells were seeded in 96-well plates at a density of  $5 \times 10^5$  per well and incubated for 24 h. Then the various concentrations (0–10000 nM) of tested compounds were added to designated wells. After 48 h incubation, medium was replaced with fresh WST-1: medium (1:10) to cell plates with 4 h in an incubator, and the absorbance of wells was read at 450 nm wavelength with VarioSkan multimode multiplate reader (Thermo Fischer Scientific). DMSO and Staurosporine treated cells were used as negative and positive controls, respectively. Cell proliferation inhibition rate of tested compounds were calculated with the following formula:

$$\text{Inhibition rate (\%)} = 100 \times (\text{OD}_{\text{control}} - \text{OD}_{\text{compound}}) / \text{OD}_{\text{control}}$$

The IC50 values of each compound in NIH-3T3 cell line were calculated by nonlinear regression (curve fit) of log concentration versus number of cells/well implemented in Prism GraphPad 5.0. statistical software (San Diego, CA) and values were represented as means ± S.E.M. from three independent experiments.

## 3. Results and discussion

### 3.1. Design

Considering the binding modes of several FGFR inhibitors in the clinic and phase stages, the strategy of the occupation of hydrophobic region I and adenine region, which are main binding sites in FGFRs, plays important for the inhibition of FGFRs (Wang et al., 2018). In our design, this strategy was based on and in addition, it was aimed to occupy other regions of the tyrosine kinase domain of FGFRs to increase selectivity and binding affinity of designed novel inhibitors at the same time. We initiated our study by choosing a proper core that has determined binding mode inside tyrosine kinase domain of FGFR1. For this purpose, the well-known FGFR inhibitor as SU4984 (13), an indolin-2-one derivative, was chosen. It was reported that indolin-2-one core of SU4984 (13) settled down into adenine region and cyclic amide atoms formed H bonds with hinge region residues as Glu562 and Ala564 in the FGFR1. In addition, it was detected that phenyl ring of SU4984 (13) made an oxygen-aromatic contact with carbonyl oxygen of Ala564 and piperazine ring of SU4984 (13) formed a van der Waals contact with Gly567 in this protein kinase (Mohammadi et al., 1997).

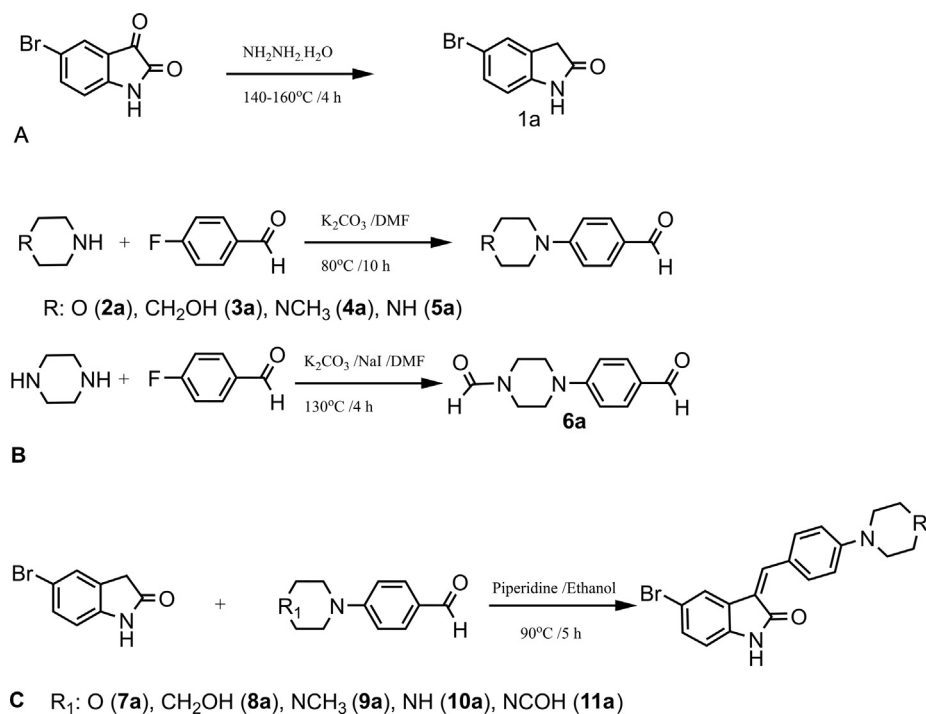
In the designing process, two approaches were carried out on SU4984 (13) to design novel FGFR inhibitors for improving selectivity and inhibitor potency on FGFRs. In the first approach, in order to occupy hydrophobic region I, there are several aromatic rings with or without various substitutions have been located at the C5 position on indolin-2-one core of SU4984 (13). The other approach which performed to SU4984 (13) is the substitution of

4-formylpiperazine ring with various rings bearing cyclic amine groups. The aim of this change is to form hydrogen bonding between amino acid residues of ATP binding sites of FGFRs and chosen rings which have hydrogen bonding acceptor and/or donor groups. Nonetheless the crystal structure of SU4984 (13) in complex with FGFR1 was determined that SU4984 (13) was *Z* isomer form inside FGFR1, but according to reported study by Sun *et al.*, SU4984 (13) was determined as *E* isomer (Mohammadi *et al.*, 1997; Sun *et al.*, 1998). Therefore, the compounds were designed and built as both *E* and *Z* isomers in order to detect their estimated binding affinities inside FGFRs using molecular modelling programs. The docking study exhibited that 4-substituted benzylidene group of *E* isomers of most of the designed compounds went towards from the nucleotide domain to the phosphate-binding region in FGFRs. This gives us to occupy nucleotide domain and phosphate-binding region in addition to adenine region. Besides it was detected that 4-substituted benzylidene group of some *E* isomers occupied hydrophobic region I. Therefore, the placing of 4-substituted benzylidene group at the C3 position of indolin-2-one could contribute either occupation of nucleotide domain and phosphate-binding region or hydrophobic region I, when the existing of aromatic groups at the C5 position of indolin-2-one core. Furthermore, locating aromatic groups at the C5 position of indolin-2-one has provided to occupation of hydrophobic region I when indolin-2-one core of designed compounds was settled down adenine region so for both isomers. Following docking study, we decided to locate  $\beta$ -naphthol, [1,1'-biphenyl]-4-ol, morpholino(phenyl)methanone, phenyl(piperidin-1-yl)methanone, phenyl(pyrrolidin-1-yl)methanone and (4-methylpiperazin-1-yl)(phenyl)methanone groups at the C5 position of indolin-2-one core and to change 4-formyl piperazine group with 4-methylpiperazine, morpholine, piperazine and 4-hydroxypiperidine groups (Fig. 2). Then, when docking study results were evaluated for designing of compounds, it was observed that preferred aromatic groups located at the C5 position of indolin-2-one occupied hydrophobic region I of FGFR1, FGFR2 and FGFR4, however, *E* isomers bearing *p*-amidophenyl groups at the C5 position of indolin-2-one displayed different bind-

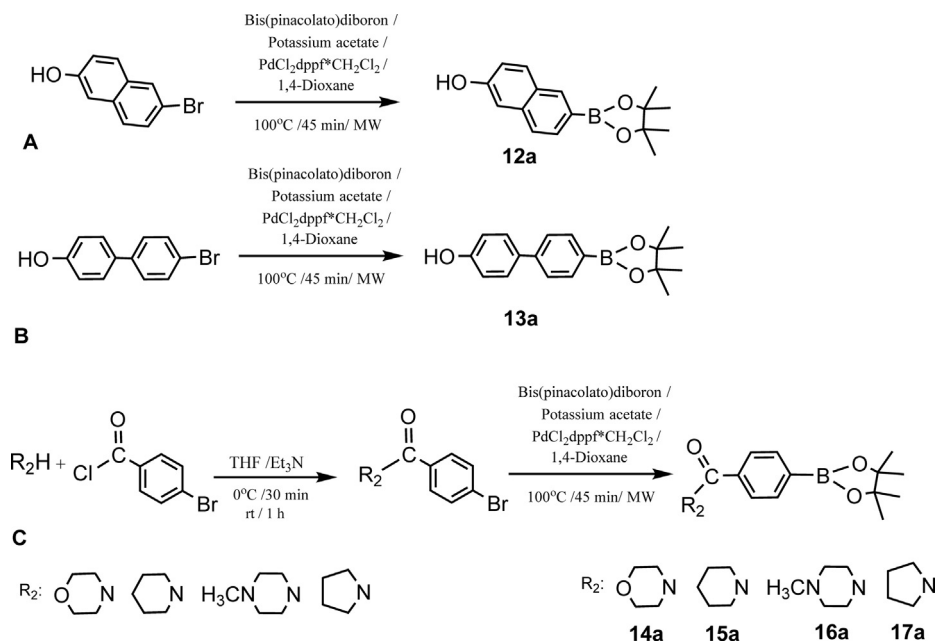
ing orientation inside homology model of FGFR3 in compare to *E* isomers bearing 6-hydroxynaphthyl and 4'-[1,1'-biphenyl] groups. It was observed that these isomers located through adenine region to phosphate-binding region of FGFR3. To verify this hypothesis, we designed and synthesized 5-substituted-3-(4-substituted benzylidene)indolin-2-one derivatives.

### 3.2. Chemistry

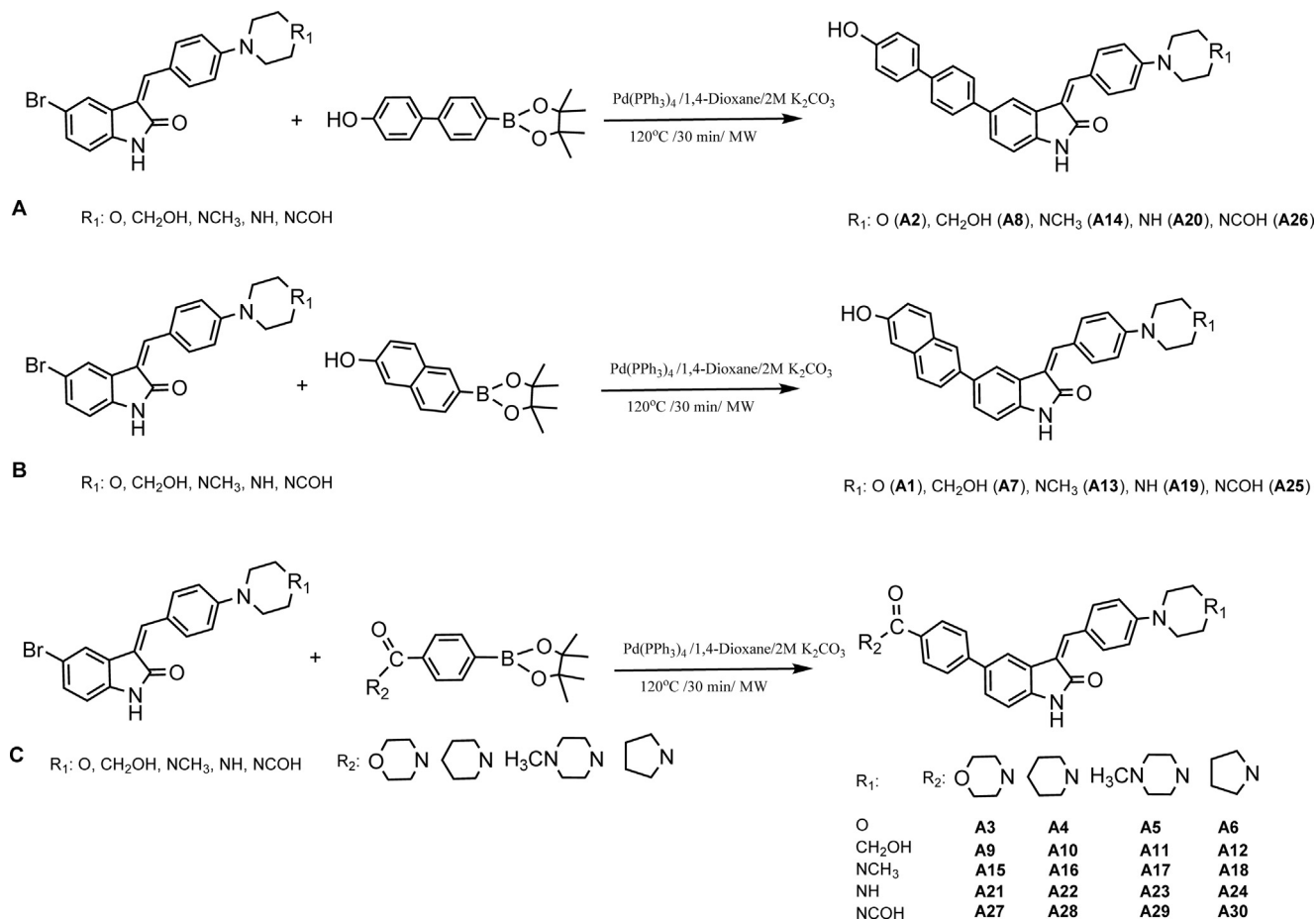
The synthetic routes of the intermedia structures and final structures were summarized in Schemes 1–3. Firstly, synthesis of 5-bromoindolin-2-one (1a) was realized by a Wolff-Kishner-like reduction of commercially available 5-bromoindolin-2-one with hydrazine hydrate (Sun *et al.*, 1998). Afterward, 4-substituted benzaldehydes (2a–5a) were prepared by 4-fluorobenzaldehyde treated with appropriate cyclic amines (morpholine, 4-hydroxypiperidine, 4-methylpiperazine and piperazine) using reported method (Beena *et al.*, 2014). Compound 6a was prepared by 4-fluorobenzaldehyde and piperazine using potassium carbonate and sodium iodide in dry DMF at 130 °C for 4 h (Scheme 1). 3-Substituted indolin-2-ones (7a–11a) were prepared by 5-bromoindolin-2-one and 4-substituted benzaldehydes (2a–6a) with piperidine in dry ethanol (Scheme 1) (Sun *et al.*, 1998). 4-Bromobenzamides were prepared by 4-bromobenzoyl chloride and appropriate cyclic amines (morpholine, piperidine, 4-methylpiperazine and pyrrolidine) under the catalytic condition of triethylamine in THF (Altman and Wilson, 2010). Boronic acid pinacol esters of 6-bromonaphthol (12a), 4-(4-bromophenyl)phenol (13a) were prepared by palladium catalysis of commercially available 6-bromonaphthalen-2-ol and 4'-bromo-[1,1'-biphenyl]-4-ol with bis(pinacolato)diboron in dioxane using microwave reactor (Scheme 2) (Treu *et al.*, 2011). Boronic acid pinacol esters of 4-bromobenzamides (14a–17a) were prepared by the synthesized 4-bromobenzamides and bis(pinacolato)diboron using same protocol (Scheme 2). Synthesis of the designed final compounds was summarized in Scheme 3. 5-Substituted-3-(4-substituted benzylidene)indolin-2-one derivatives were prepared by



**Scheme 1.** Synthesis pathway for (A) 5-Bromoindolin-2-one, (B) 4-Substituted benzaldehydes and (C) 5-Bromo-3-(4-substituted benzylidene)indolin-2-ones.



**Scheme 2.** Synthesis pathway for (A) 6-Hydroxynaphthylboronic acid pinacol ester, (B) 4'-Hydroxy-[1,1'-biphenyl]boronic acid pinacol ester and (C) 4-Substituted amidophenylboronic acid pinacol esters.



**Scheme 3.** Synthesis pathway for (A) 5-(4'-Hydroxy-[1,1'-biphenyl]-4-yl)-3-(4-substituted benzylidene)indolin-2-ones, (B) 5-(6-Hydroxynaphthalen-2-yl)-3-(4-substituted benzylidene)indolin-2-ones and (C) 5-(4-Substituted amidophenyl)-3-(4-substituted benzylidene)indolin-2-ones.



palladium catalysis of 5-bromo-3-(4-substituted benzylidene)indolin-2-ones (**7a-11a**) and the appropriate boronic acid pinacol esters (**12a-17a**) in 1,4-dioxane under Suzuki coupling conditions using microwave reactor (Treu et al., 2011).

The structures of title compounds were confirmed by spectral analysis as FT-IR,  $^1\text{H}$  NMR,  $^{13}\text{C}$  NMR, 2D NMR experiments ( $^1\text{H}$ - $^1\text{H}$ COSY, HSQC, HMBC ve NOESY) and ESI-Mass, and elemental analysis. In the IR spectra of title compounds, C=O stretching bands belong to indolin-2-one core and benzamides were observed at 1679–1706  $\text{cm}^{-1}$ . C=C stretching bands were observed at 1617–1673  $\text{cm}^{-1}$  (symmetric) and 1585–1607  $\text{cm}^{-1}$  (asymmetric). In addition, N–H and/or O–H stretching bands at 3160–3496  $\text{cm}^{-1}$ , C–H stretching bands at 2800–2987  $\text{cm}^{-1}$  and C–N stretching bands at 1048–1241  $\text{cm}^{-1}$  were observed. The mass spectra of title compounds were recorded by positive ion mode electrospray ionization (ESI+) technique. The  $[\text{M} + \text{H}]^+$  ions of title compounds are in complete agreement with calculated molecular weights. The purity levels of compounds were determined by elemental analysis (C, H, N) and results were within 0.4% of calculated values.  $^1\text{H}$  NMR spectra of the compounds verified existence of expected numbers of protons, and chemical shifts, multiplicities and coupling constants were also used to prove integrity and intramolecular vicinity of synthesized molecular structures.  $^{13}\text{C}$  NMR spectra and 2D NMR experiments also supported structural confirmations. The configurations of some of the reference compounds were detected using NOESY experiment, whilst configurations of the remaining compounds were appointed by comparison of their  $^1\text{H}$  NMR spectrum with those of reference compounds. Spectral and elemental analysis data of the synthesized compounds with melting points were given in [Supplementary Materials](#).

According to  $^1\text{H}$  NMR analysis results, most of 5-substituted-3-(4-substitutedbenzylidene)indolin-2-ones were determined as *E* isomer form and isomer mixture that the *E* isomer is predominant. Most of 3-(4-(piperazin-1-yl)benzylidene)indolin-2-one derivatives were detected at equilibrium between the *E* and *Z* isomer form or in slightly *Z* isomer was predominant. Two isomer forms were distinguished by 2D NOESY technique. The NOE effect between proton at the C4 position of indol-2-one and vinyl proton was observed in *Z* configured compounds, on the other hand, *E* configured compounds could display this effect between proton at the C4 position of indol-2-one and protons of phenyl ring of benzylidene group in NOESY experiment. This experiment demonstrated that chemical shifts of the proton at the C4 position were observed around at 8 ppm in for both isomers. Besides, it was observed that chemical shift values of protons of phenyl ring of benzylidene group and vinyl proton were found different for *E* and *Z* configured compounds. For instance, chemical shifts of protons at the C2' and C6' position of phenyl ring of benzylidene group were observed around 7.66–7.72 ppm for the *E* isomers but 8.41–8.47 ppm for the *Z* isomers. In the *E* isomers, chemical shifts of vinyl protons were detected around 7.57 ppm, while, these were detected around 7.85 ppm for the *Z* isomers. The chemical shifts of vinyl protons and protons at the C2' and C6' position of synthesized compounds for both *E* and *Z* isomers, and % of isomers were given in [Table 1](#).

### 3.3. Biological activity

The FGFR inhibitory potencies and selectivity of synthesized compounds were determined by using FRET-Base Z'-Lyte biochemical kinase assay. Staurosporin was used as a positive control to screening conditions. The results of enzyme inhibition study and selectivity index values were summarized and reported in [Table 2](#) and [Table 3](#), respectively. Besides, cytotoxicity potency of title compounds was evaluated by *in vitro* cell culture study using NIH-3T3 cell line with WST-1 cell proliferation reagent.

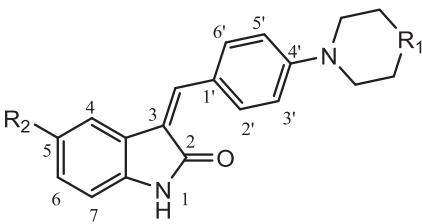
According to enzyme inhibition assay, there are only six compounds among the synthesized compounds that displayed inhibitory potency on FGFR2 in the studied concentration range. Otherwise, all synthesized compounds displayed inhibitory potency against FGFR1, FGFR3 and FGFR4 with several  $\text{IC}_{50}$  values in the studied concentration range. Especially, they were found in efficient to inhibition of FGFR1 and FGFR3 with low  $\text{IC}_{50}$  values in comparison to FGFR4. Title compounds displayed FGFR1 inhibitory potency with  $\text{IC}_{50}$  values between 6.996 nM and 9.129  $\mu\text{M}$ . Compound **A13** was found as the best FGFR1 inhibitor with an  $\text{IC}_{50}$  value of 6.996 nM among the studied compounds additionally, it was also highly selective on FGFR1. It has displayed inhibitory potency against FGFR2, FGFR3 and FGFR4 with  $\text{IC}_{50}$  values of 1.022  $\mu\text{M}$ , 17.09  $\mu\text{M}$  and 8.993  $\mu\text{M}$ , respectively. Besides, other compounds which have better inhibitory potency against FGFR1 are in descending order as compound **A21**, compound **A23** and compounds **A8** ([Table 2](#)). As a result of enzyme inhibition assay, only four compounds have displayed inhibitory potency against FGFR1 with  $\text{IC}_{50}$  values over 1  $\mu\text{M}$ . The compounds bearing *N*-methylpiperazine and 4-hydroxypiperidin groups at the C4' position have showed inhibitory potency with  $\text{IC}_{50}$  value less than 1  $\mu\text{M}$  against FGFR1. Among the compounds bearing *N*-methylpiperazine and 4-hydroxypiperidin groups at the C4' position, the compounds bearing 6-hydroxynaphthalene and 4'-hydroxy-(1,1'-biphenyl) groups at the C5 position displayed inhibitory potency  $\text{IC}_{50}$  values less than 16 nM against FGFR1. It was observed that compound **A19** ( $\text{IC}_{50}$  = 1.106  $\mu\text{M}$  for FGFR1) and compound **A25** ( $\text{IC}_{50}$  = 3.976  $\mu\text{M}$  for FGFR1) have poor inhibitory potency against FGFR1 in comparison to other compounds bearing 6-hydroxynaphthalene and 4'-hydroxy-(1,1'-biphenyl) groups at the C5 position. In addition, the compounds bearing *p*-amidophenyl groups at the C5 position have displayed high to moderate inhibitory activity against FGFR1 excluded compound **A5** ( $\text{IC}_{50}$  = 1.89  $\mu\text{M}$  for FGFR1) and compound **A29** ( $\text{IC}_{50}$  = 9.129  $\mu\text{M}$  for FGFR1). Among the *p*-amidophenyl derivatives, the compounds bearing piperazine groups at the C4' position exhibited very good inhibitory activity against FGFR1 with the  $\text{IC}_{50}$  values between 9.544 nM and 92.4 nM.

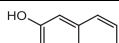
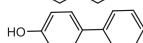
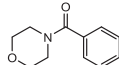
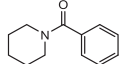
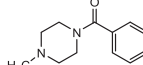
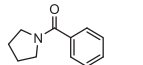
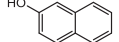
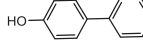
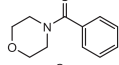
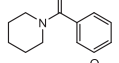
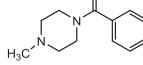
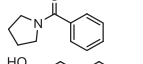
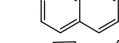
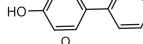
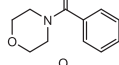
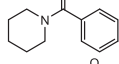
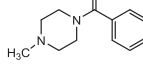
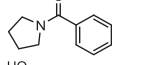
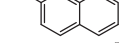
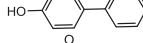
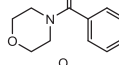
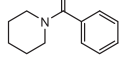
Compound **A1** displayed the best inhibitory potency with an  $\text{IC}_{50}$  value of 5.946 nM and high selectivity against FGFR2. This has 3.3-fold, 238.6-fold and 6247.9-fold better inhibitory potency than against FGFR1, FGFR3, and FGFR4, respectively, in compare to FGFR2. Besides, the compounds bearing morpholine and 4-hydroxypiperidin groups at the C4' position, and 6-hydroxynaphthalene and 4'-hydroxy-(1,1'-biphenyl) groups at the C5 position have high inhibitory potency with  $\text{IC}_{50}$  value less than 12 nM against FGFR2.

Compound **A5** showed the best inhibitory potency against FGFR3 with an  $\text{IC}_{50}$  values of 6.501 nM. The most of compounds (included compound **A5**) bearing *p*-amidophenyl groups at the C5 position of indolin-2-one displayed inhibitory potency with  $\text{IC}_{50}$  value less than 200 nM against FGFR3. Especially, the *p*-amidophenyl derivatives such as the compounds bearing *N*-methylpiperazine and 4-hydroxypiperidin groups at the C4' position have encouraging inhibitory potency against FGFR3 ([Table 2](#)). Excluded compound **A11** ( $\text{IC}_{50}$  = 105.6 nM for FGFR3) and compound **A18** ( $\text{IC}_{50}$  = 155.7 nM for FGFR3), these derivatives showed inhibitory potency with  $\text{IC}_{50}$  value less than 40 nM against FGFR3. Subsequent to compound **A5** bearing morpholine group at the C4' position and *p*-[(4-methylpiperazine)carbonyl]phenyl group at the C5 position, compound **A16** ( $\text{IC}_{50}$  = 14.27 nM) and compound **A17** ( $\text{IC}_{50}$  = 13.32 nM) have better inhibitory against FGFR3, among the *p*-amidophenyl derivatives. Otherwise, the compounds bearing 6-hydroxynaphthalene and 4'-hydroxy-(1,1'-biphenyl) groups at the C5 position of indolin-2-one displayed moderate to low inhibitory activity against FGFR3 excluded compound **A20** that has second best inhibitory potency with  $\text{IC}_{50}$  values of 6.767 nM, and com-

**Table 1**

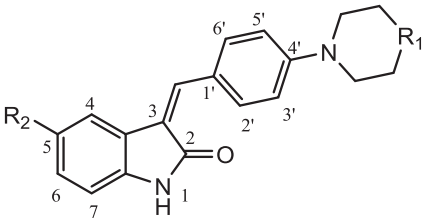
Chemical formula of the synthesized A series compounds and their preferred configurations determined by NMR experiments.

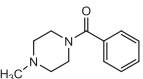
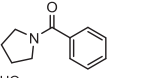
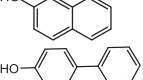
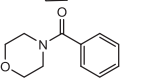
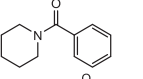
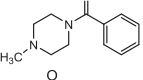
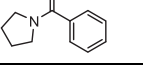
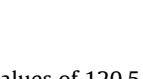


Compound ID	Substitutions		NMR data chemical shift in ppm				% of E isomer	% of Z isomer
	R1	R2	E isomer H2'-H6'	Z isomer H2'-H6'	E isomer H-vinyl	Z isomer H-vinyl		
A1	O		7.72	8.47	7.58	Nd*	96	4
A2	O		7.66	8.47	7.58	7.87	97	3
A3	O		7.70	8.45	7.58	7.86	98	2
A4	O		7.70	8.45	7.58	7.86	96	4
A5	O		7.68	8.45	7.58	7.86	98	2
A6	O		7.69	8.46	7.59	7.87	91	9
A7	CHOH		7.77	8.47	7.58	7.86	35	65
A8	CHOH		7.66	8.45	7.57	7.83	70	30
A9	CHOH		7.67		7.55		100	
A10	CHOH		7.67		7.56		100	
A11	CHOH		7.65		7.56		100	
A12	CHOH		7.65		7.56		100	
A13	NCH <sub>3</sub>		7.70–7.72	8.49	7.57	7.85	92	8
A14	NCH <sub>3</sub>		7.70	8.45	7.57	7.85	71	29
A15	NCH <sub>3</sub>		7.67		7.57		100	
A16	NCH <sub>3</sub>		7.67		7.57		100	
A17	NCH <sub>3</sub>		7.66		7.57		100	
A18	NCH <sub>3</sub>		7.66		7.57		100	
A19	NH		7.77	8.47	7.58	7.86	60	40
A20	NH		7.59–7.69	8.41–8.47	7.59–7.69	7.84	50	50
A21	NH		7.69	8.44	7.57	7.84	38	62
A22	NH		7.69	8.44	7.57	7.84	45	55

(continued on next page)

Table 1 (continued)



Compound ID	Substitutions		NMR data chemical shift in ppm				% of E isomer	% of Z isomer
	R1	R2	E isomer H2'-H6'	Z isomer H2'-H6'	E isomer H-vinyl	Z isomer H-vinyl		
A23	NH		7.69	8.44	7.57	7.84	45	55
A24	NH		7.68	8.44	7.57	7.84	50	50
A25	NCHO		7.72	8.48	7.58	Nd*	99	1
A26	NCHO		7.70	8.47	7.59	7.86	97	3
A27	NCHO		7.70	8.45	7.58	7.86	97	3
A28	NCHO		7.71	8.46	7.58	7.86	93.5	6.5
A29	NCHO		7.70	8.45	7.58	Nd*	99	1
A30	NCHO		7.70	8.45	7.58	7.85	98	2

Nd\*: Not determined.

Compound **A19** with  $IC_{50}$  values of 120.5 nM. It was detected that they have inhibitory potency against FGFR3 with the  $IC_{50}$  values between 481.2 nM and 17.09  $\mu$ M.

According to *in vitro* enzyme inhibition assay, the synthesized compounds displayed very low inhibitory activity against FGFR4 in comparison with other isoforms. Only a compound displayed inhibitory activity less than 1  $\mu$ M (Table 2). Compound **A6** bearing morpholine group at the C4' position and *p*-(pyrrolidinecarbonyl) phenyl group at the C5 position showed the best inhibitory potency against FGFR4 with an  $IC_{50}$  values of 822.8 nM. It was observed that other indolin-2-ones displayed inhibitory potency against FGFR4 with the  $IC_{50}$  values between 3.67  $\mu$ M and 37.15  $\mu$ M.

Considering FGFR selectivity of studied compounds, there are seven compounds (**A6**, **A13**, **A14**, **A18**, **A21**, **A22** and **A23**) displayed selectivity to FGFR1, while two compounds (**A1** and **A2**) for FGFR2, and nine compounds (**A3**, **A5**, **A9**, **A10**, **A12**, **A16**, **A17**, **A19** and **A20**) for FGFR3. Besides, two compounds (compound **A7** and **A8**) showed selectivity to FGFR1 and FGFR2, and four compounds (compound **A4**, **A11**, **A15** and **A24**) showed selectivity to FGFR1 and FGFR3.

NIH-3T3 cells are the mouse embryonic fibroblast cells which express endogenous FGFR1 and FGFR2 in physiological level (Garcia-Maya et al., 2006). According to *in vitro* cell culture study that was performed to determine cytotoxic potential of synthesized compounds against NIH-3T3 cells, compound **A24** exhibited highest cytotoxicity with  $IC_{50}$  value of 180.1 nM. While other compounds which exhibited cytotoxicity against NIH-3T3 cells are in descending order as compound **A22** ( $IC_{50}$  = 210.6 nM) and compound **A19** ( $IC_{50}$  = 282.7 nM), and also eight compounds displayed

cytotoxicity less than  $IC_{50}$  value of 1  $\mu$ M. Compound **A24**, **A22** and **A19** bearing piperazine group at the C4' position displayed FGFR1 inhibition with  $IC_{50}$  values of 92.4 nM, 18.28 nM and 1.106  $\mu$ M, respectively. Other compounds which exhibited cytotoxicity against NIH-3T3 cells are in descending order as compound **A4** ( $IC_{50}$  = 399.7 nM), compound **A16** ( $IC_{50}$  = 626 nM), compound **A6** ( $IC_{50}$  = 818.3 nM), compound **A28** ( $IC_{50}$  = 839.1 nM), compound **A2** ( $IC_{50}$  = 949.4 nM) and compound **A10** ( $IC_{50}$  = 983.2 nM), and they displayed FGFR1 inhibition less than with  $IC_{50}$  values of 350 nM (Table 2). On the other hand, the compounds (**A1**, **A7** and **A8**) which have FGFR1 and FGFR2 inhibitory potency, displayed cytotoxicity against NIH-3T3 cells with  $IC_{50}$  values between 1.577  $\mu$ M and 18.56  $\mu$ M. In addition, compound **A13**, **A14**, **A21**, **A23** and **A27** which displayed FGFR1 inhibition less than with  $IC_{50}$  values of 16 nM, exhibited cytotoxicity against NIH-3T3 cells with  $IC_{50}$  values over 1  $\mu$ M. These data of *in vitro* cell culture study showed that the cytotoxicity against NIH-3T3 cells was not only due to the inhibition of FGFR1 or FGFR1-2. The results of the cytotoxicity study were summarized and reported in Table 2.

### 3.4. Molecular modelling

#### 3.4.1. Docking study

Molecular docking is powerful tool that determines interactions between small molecule candidates and their target proteins theoretically. In this study, this technique was used to help of designing of candidates of novel FGFR inhibitors and to determine binding orientations of synthesized indolin-2-one derivatives inside FGFRs. In advance of docking study, proteins and studied compounds were

**Table 2***In vitro* inhibition of FGFRs and cytotoxicity of synthesized compounds against NIH-3T3 Cells.

Compounds	FGFR1-IC <sub>50</sub> (nM)	FGFR2-IC <sub>50</sub> (nM)	FGFR3-IC <sub>50</sub> (nM)	FGFR4-IC <sub>50</sub> (nM)	NIH-3T3 Cells IC <sub>50</sub> (nM)
Staurosporin	2.078 ± 0.722	1.196 ± 0.211	54.135 ± 4.371	255.87 ± 37.83	39.03 ± 2.279
A1	19.82 ± 3.318	5.946 ± 0.407	1419 ± 422.797	37150 ± 964.8	1577 ± 171.4
A2	218.9 ± 4.324	8.436 ± 0.237	3457 ± 510.343	21210 ± 350.7	949.4 ± 24.72
A3	685.6 ± 27.712	Nd*	52.519 ± 4.705	3670 ± 290.5	3257 ± 121.1
A4	107.1 ± 3.841	Nd*	194.83 ± 5.612	15120 ± 313.3	399.7 ± 100.2
A5	1890 ± 43.433	Nd*	6.501 ± 0.436	18590 ± 208.8	2751 ± 308.2
A6	49.02 ± 0.688	Nd*	1093 ± 47.317	822.8 ± 107.5	818.3 ± 240.6
A7	15.44 ± 0.442	11.94 ± 1.336	8131 ± 471.822	18580 ± 172.5	18560 ± 1847
A8	10.78 ± 3.727	6.988 ± 0.603	6433 ± 486.836	27140 ± 276.9	2227 ± 206.8
A9	64.45 ± 1.232	Nd*	19.128 ± 3.218	17740 ± 328.5	1145 ± 219.6
A10	344.7 ± 3.411	Nd*	17.229 ± 0.419	23150 ± 271.1	983.2 ± 158.31
A11	154.6 ± 6.175	Nd*	105.6 ± 2.805	20210 ± 259	87790 ± 4294.6
A12	645.6 ± 10.941	Nd*	22.48 ± 0.737	4895 ± 402	4960 ± 187.3
A13	6.996 ± 0.206	1022 ± 67.304	17090 ± 294.321	8993 ± 314.3	30070 ± 3233
A14	14.927 ± 0.436	6970 ± 139.138	4855 ± 480.203	19820 ± 121.8	18660 ± 368.3
A15	38.711 ± 0.504	Nd*	38.83 ± 1.347	14810 ± 448.7	9500 ± 260.5
A16	255.7 ± 28.123	Nd*	14.17 ± 2.119	15050 ± 64.14	626 ± 140.2
A17	819.8 ± 3.631	Nd*	13.32 ± 2.931	7228 ± 288.2	4699 ± 105.1
A18	49.17 ± 2.517	Nd*	155.7 ± 31.343	14530 ± 211.1	2542 ± 146.4
A19	1106 ± 35.768	Nd*	120.5 ± 23.084	13580 ± 236.1	282.7 ± 158.3
A20	72.17 ± 4.321	Nd*	6.767 ± 0.336	18040 ± 687.9	1442 ± 249.4
A21	9.544 ± 0.313	Nd*	4512 ± 311.125	28130 ± 974	2646 ± 202.7
A22	18.28 ± 0.627	Nd*	565.7 ± 6.737	26770 ± 186.8	210.6 ± 143.7
A23	10.03 ± 0.908	Nd*	56.518 ± 0.308	8479 ± 330.6	1580 ± 301.9
A24	92.4 ± 1.131	Nd*	162.9 ± 7.216	13840 ± 478.3	180.1 ± 20.6
A25	3976 ± 0.354	Nd*	1087 ± 477.12	6132 ± 208.1	24510 ± 305.8
A26	422 ± 40.308	Nd*	481.2 ± 24.109	10140 ± 322	2502 ± 267.5
A27	11.956 ± 0.736	Nd*	131.1 ± 4.228	9238 ± 265.4	1226 ± 467.4
A28	77.27 ± 3.142	Nd*	33.61 ± 0.574	7032 ± 243.5	839.1 ± 232.2
A29	9129 ± 1762	Nd*	187 ± 4.117	6101 ± 347.1	10140 ± 250.7
A30	67.189 ± 2.917	Nd*	193.5 ± 39.326	6325 ± 322.2	1594 ± 224.3

Nd\*: Not determined.

**Table 3**Selectivity index values of the studied compounds for *in vitro* inhibition of FGFRs.

Compounds	FGFR1-SI	FGFR2-SI	FGFR3-SI	FGFR4-SI
A1	3.333	1	238.648	6247.898
A2	25.948	1	409.791	2514.228
A3	13.054	–	1	69.878
A4	1	–	1.819	141.176
A5	290.725	–	1	2859.560
A6	1	–	22.297	16.785
A7	1.293	1	680.988	1556.114
A8	1.543	1	920.578	3883.801
A9	3.369	–	1	927.339
A10	20.006	–	1	1343.587
A11	1.464	–	1	191.383
A12	28.719	–	1	217.749
A13	1	146.083	2442.824	1285.449
A14	1	464.667	323.667	1321.333
A15	1	–	1.003	382.588
A16	17.919	–	1	1054.660
A17	61.547	–	1	542.643
A18	1	–	3.167	295.505
A19	9.178	–	1	2006.798
A20	10.665	–	1	2665.879
A21	1	–	472.758	2947.402
A22	1	–	30.946	1464.442
A23	1	–	5.635	845.364
A24	1	–	1.763	149.784
A25	3.658	–	1	5.641
A26	1	–	1.14	24.028
A27	1	–	10.962	77.241
A28	2.299	–	1	209.223
A29	48.818	–	1	32.626
A30	1	–	2.880	94.136

\*Selectivity index of each compound was calculated by IC<sub>50</sub>/IC<sub>50</sub>. Lowest IC<sub>50</sub> value is accepted as 1 unit for each compound.

prepared by procedures given in materials and methods section. The docking scores of suggested binding poses were calculated inside FGFRs with GOLD 5.2.1 software using GoldScore scoring function and reported in Table 4 (Jones et al., 1995).

Molecular docking technique was performed during design process of synthesized compounds. In the docking study which performed before synthesis and enzyme inhibition assay, it was observed that indolin-2-one core of both *E* and *Z* isomers of designed compounds settled down into adenine binding site of ATP in general, and aromatic systems at the position 5 of indolin-2-one core occupied hydrophobic region I of FGFR1, FGFR2 and FGFR4 in particular. On the other hand, it was detected that 6-hydroxynaphthyl and 4'-hydroxy[1,1'-biphenyl] groups of designed compounds occupied hydrophobic region I of FGFR3. Considering enzyme inhibition assay, only six of synthesized compounds have inhibitory potencies against FGFR2 in particular, and this has suggested that most of designed compounds haven't occupied ATP binding site in FGFR2. Besides, the suggested binding poses of synthesized compounds have been proposed after evaluation of results of enzyme inhibition assays. It has been thought that the compounds, which have high inhibitory potency on related FGFRs, settled down in these FGFRs in accordance with design hypothesis. After biological activity studies, though it was found that synthesized compounds have low affinity to FGFR4 in comparison to other FGFRs, calculated docking scores of compounds inside FGFR4 have been found higher than other isoforms in general. The suggested binding poses of synthesized compounds inside FGFRs were given in Tables S2–S5 inside [supplementary materials](#) section with calculated docking scores.

According to the results of enzyme inhibition assay, compound **A1**, **A5** and **A13** have displayed best inhibitory potency against FGFR2, FGFR3 and FGFR1 among the synthesized compounds, respectively. When the suggested binding pose of compound **A1** obtained from docking study was evaluated, it was observed that



**Table 4**  
Docking scores for the synthesized compounds inside FGFR1 (PDB id: 5B7V), FGFR2 (PDB id: 3R11), FGFR3 (Homology model) and FGFR4 (PDB id: 4QRC) using Goldscore.

Compounds	FGFR1	FGFR2	FGFR3	FGFR4
A1	74.6729 (17)	75.1803 (2)	73.9352 (9)	76.3455 (64)
A2	68.0593 (6)	72.9544 (2)	73.2571 (15)	74.6141 (17)
A3	62.2323 (7)	74.4287 (1)	75.8768 (1)	70.5575 (8)
A4	60.4480 (5)	72.4071 (9)	75.4875 (6)	74.1584 (1)
A5	59.4395 (5)	74.2727 (6)	78.1142 (1)	71.1945 (5)
A6	68.3380 (2)	76.0021 (1)	74.6522 (13)	77.2019 (6)
A7/E	74.1791 (29)	70.8265 (5)	75.9941 (12)	71.5228 (62)
A7/Z	69.8491 (7)	75.1318 (7)	68.6276 (7)	80.2975 (36)
A8/E	74.1934 (2)	77.9072 (1)	75.8564 (4)	74.1330 (26)
A8/Z	68.4744 (6)	71.2654 (4)	70.4308 (8)	80.7514 (3)
A9	65.6469 (5)	70.5121 (3)	72.2507 (1)	66.9305 (25)
A10	63.6817(4)	69.8373 (7)	75.9743 (1)	69.2663 (10)
A11	60.7540 (5)	75.6790 (6)	73.1754 (3)	69.5999 (12)
A12	65.4059 (9)	69.9169 (9)	75.2554 (5)	75.6089 (2)
A13	83.7696 (1)	73.6600 (2)	75.4410 (13)	74.9924 (60)
A14/E	71.2330 (1)	71.7616 (2)	73.0279 (13)	69.8318 (30)
A14/Z	69.3618 (1)	79.1050 (1)	66.7284 (26)	81.7560 (2)
A15	68.6760 (1)	77.1553 (1)	78.6265 (9)	72.8380 (2)
A16	67.2630 (2)	71.8328 (1)	78.8878 (16)	70.9715 (5)
A17	64.1258 (10)	73.3599 (7)	81.4977 (2)	79.2981 (2)
A18	71.0470 (2)	74.7267 (3)	79.6453 (9)	74.5521 (11)
A19/E	66.5366 (40)	76.7998 (1)	76.3253 (8)	78.5124 (55)
A19/Z	66.1633 (20)	78.7914 (1)	69.5999 (1)	82.7722 (8)
A20/E	72.1175 (1)	74.6526 (1)	78.8802 (1)	73.5924 (40)
A20/Z	69.4367 (1)	59.5031 (86)	69.5444 (4)	81.5669 (4)
A21/E	66.4417 (3)	73.8033 (5)	74.3847 (12)	74.0508 (3)
A21/Z	66.3429 (2)	72.9884 (1)	66.4909 (1)	86.6189 (1)
A22/E	73.2875 (1)	72.3509 (21)	74.0136 (15)	70.9649 (11)
A22/Z	63.2021 (4)	67.9133 (7)	66.6112 (1)	88.0003 (1)
A23/E	64.9942 (4)	75.3031 (6)	77.5348 (5)	75.3620 (5)
A23/Z	63.6466 (4)	75.0663 (1)	67.0567 (1)	78.8071 (62)
A24/E	67.0052 (4)	73.1923 (8)	76.2699 (5)	75.5954 (8)
A24/Z	63.6398 (9)	68.7747 (10)	68.0912 (1)	85.7332 (2)
A25	62.8397 (73)	76.8138 (2)	75.4431 (20)	71.5370 (57)
A26	72.3057 (55)	63.2505 (36)	77.2216 (6)	68.8704 (34)
A27	72.3088 (3)	67.5403 (8)	76.9574 (10)	75.9336 (1)
A28	71.0663 (10)	75.8122 (1)	79.3010 (3)	73.1431 (7)
A29	65.7827 (27)	70.6836 (8)	75.7519 (14)	79.8302 (2)
A30	68.8331 (5)	74.4726 (5)	75.9175 (9)	76.6699 (3)

The absolute ranking positions for the suggested binding poses were given inside brackets.

indolin-2-one core have settled down into adenine binding region of ATP. Besides, 6-hydroxy naphthalene ring at C5 position has occupied hydrophobic region I inside FGFR2. Lastly, 4-morpholinobenzylidene group at the C3 position occupied a cleft formed by amino acid residues such as Glu489, Gly490, Cys491, Phe492, and Gly493, that over phosphate binding region of ATP, inside FGFR2 (Fig. 3).

Regarding the suggested binding pose of compound **A13** inside FGFR1, indolin-2-one core and 6-hydroxy naphthalene ring at C5 position have settled down into adenine binding region of ATP and hydrophobic region I, respectively. Especially, amide group of indolin-2-one core has arrived to hinge region of adenine binding region of ATP formed by Glu562, Tyr563 and Ala564. In addition, 4-(4-methylpiperazin-1-yl)benzylidene group at the C3 position has lied onto the phosphate binding region of ATP inside FGFR1 and occupied a cleft formed by amino acid residues such as Leu484, Gly485, Glu486, Glu489, Gly490, Gln491, and Val492 (Fig. 3).

Considering the suggested binding pose of compound **A5** inside FGFR3, title compound has settled into FGFR3 with different orientation as compare with compound **A1** in FGFR2 and compound **A13** in FGFR1. It was observed that 4-methylpiperazinamido group at the C5 position has located between Asn562 and Leu478 in the nucleotide binding domain of ATP. Besides, indolin-2-one core of compound **A5** has settled into a pocket formed by amino acid residues of phosphate binding region as Gly484, Lys508, Asp521 and Leu522, and 4-morpholinobenzylidene group at the C3 position has located between amino acid residues as Phe483, Asp617 and Arg655 (Fig. 3).

The suggested binding poses of all three compounds in related proteins that evaluated in this section were used as initial structures for investigating of protein-ligand interactions with MD simulations (Fig. 3).

### 3.4.2. Molecular dynamics simulations

Molecular dynamics simulations are an efficient technique that was used to evaluate dynamics behaviors between drug candidates and their related proteins in contrast to molecular docking studies using a single conformation in general. In the current study, there are three compounds **A1**, **A5** and **A13** which showed best inhibitor potency against FGFR2, FGFR1 and FGFR3, respectively, were chosen to evaluate dynamics behaviors inside their related proteins using structural stability analysis, binding mode analysis and free binding energy calculations. The conformations of these compounds inside their related proteins obtained using GOLD 5.2.1 software were selected to use generating of MD simulations. The protein-ligand complexes and apo forms were prepared by the procedure mentioned in the materials and methods section and were exposed to free MD simulations though 100 ns after equilibrium step.

**3.4.2.1. Structural stability analysis.** In this study, when the RMSD plot of compound **A1**-FGFR2, compound **A5**-FGFR3 and compound **A13**-FGFR1 complexes obtained from MD simulations were evaluated it was seen that title compounds were kept their stabilities inside their related proteins during whole MD simulations. In the RMSD plot of compound **A1**-FGFR2 complex, it was observed that

the average RMSD value of compound **A1**-FGFR2 complex was around 1.5 Å in the first period as 53 ns and it gradually increased around 1.5 Å to 2.5 Å between 53 ns and 82 ns. Then, it decreased to around 2.0 Å at the end of MD simulations. In addition, the average RMSD value of compound **A1** was observed at around 0.1 Å during entire MD simulations (Fig. 4). In the MD simulations of compound **A1**-FGFR2 complex, the trajectory of complex suggested that the key interactions formed between ligand and protein were preserved and ligand kept its orientation inside protein with minimal changing (Fig. S1). After the 80 ns, even though the interactions between ligand and protein weakened in the short period, they have become strengthen at the end of the MD simulation.

According to the RMSD plot of compound **A5**-FGFR3 complex, the average RMSD value of complex was observed as increased around 2.0 Å to 5.0 Å at the time slot of 0 ns and 5 ns. The average RMSD value was displayed as fluctuated between around 4.5 Å and 5.0 Å at the rest of MD simulations. The average RMSD value of compound **A5** was observed at around 0.1 Å during entire MD simulations (Fig. 4). The MD trajectory of complex displayed that the binding orientation of ligand was conserved during the whole MD simulation with preserving key interactions inside FGFR3 (Fig. S2). Especially, the salt bridge formed with Asp635 and compound **A5** was conserved during the entire MD simulation (Fig. S3, Fig. S4).

In the RMSD plot of compound **A13**-FGFR1 complex, the average RMSD value was observed as increased around 3.0 Å to 5.5 Å at the time slot of 0 ns and 32 ns. After 32 ns, it increased to around 3.5 Å and fluctuated between around 3.5 Å and 5.0 Å during 50 ns, and the average RMSD value of complex remained stable around 3.5 Å after 83 ns. The average RMSD value of compound **A13** was determined at around 0.1 Å during entire MD simulations (Fig. 4). The MD trajectory of complex was observed that the RMSD value increased rapidly at the significant time slots and decreased the same values during the 83 ns. This considered that the interactions weakened between the protein and ligand during these time periods. On the other hand, it was displayed that compound **A13** has kept its binding orientation inside FGFR1 (Fig. S5). Especially, hydrogen bonding formed with ligand and Glu531 that is the residue of hydrophobic pocket I (Table S6). But it was considered that the expanding of the ribose and phosphate-binding regions of FGFR1 due to the mobility of amino acid residues during the MD simulations caused the weakened interactions between ligand and residues and the occurring of these sharp fluctuations (Fig. S5).

Regarding the RMSD plots of apo forms of title proteins, the average RMSD value of apo form of FGFR2 was observed between around 1.5 Å and 2.0 Å during whole MD simulations. The average RMSD value of apo form of FGFR3 was viewed as fluctuated between around 2.5 Å and 4.0 Å in the first part of free MD simulations, and as fluctuated between around 3.5 Å and 4.5 Å at the rest of MD simulations. In the RMSD plots of apo form of FGFR1, the average RMSD value was observed around 2.0 Å during entire MD simulations even if it rose around 3.0 Å in short time slots (Fig. 4).

**3.4.2.2. Binding mode analysis.** Hydrogen bonding network plays important key role in the binding between ligand and its target protein. In our study, the geometry and stability of hydrogen bonding network in compound **A1**-FGFR2, compound **A5**-FGFR3 and compound **A13**-FGFR1 complexes were detected with analysis of MD simulations of title complexes.

According to binding mode analysis results of compound **A1**-FGFR2 complexes, compound **A1** formed hydrogen bonds with backbone amino acid residues and water molecules inside the active site, and formed water-mediated hydrogen bonds with backbone amino acid residues (Tables S6–S8). The hydroxyl group on the naphthalene ring of compound **A1** formed hydrogen bonds

with carboxylate group of Glu534, amide group in the indolin-2-one ring formed a hydrogen bond with carbonyl group of Ala567 and oxygen atom of morpholine ring of compound **A1** formed a hydrogen bond with p-loop amino acid residue as Phe492 (Table S6). Besides, compound **A1** formed hydrogen bonds with water molecules inside ATP binding region and p-loop of FGFR2 (Table S7, Fig. S1). Water-mediated hydrogen bonds were observed between compound **A1** and ATP binding region amino acid residues as Tyr566, Ala567, Ser568 and Asp644 (Table S8). In addition to hydrogen bonds, CH- $\pi$  and hydrophobic interactions contributed binding motif of compound **A1** inside FGFR2. The naphthalene ring of compound **A1** settled down inside hydrophobic region I formed hydrophobic interactions with amino acid residues of this region and the CH- $\pi$  interactions with alkyl side chains of hydrophobic region I amino acid residues. In addition, hydrophobic interactions also were formed by p-morpholinophenyl group of compound **A1** and hydrophobic cleft residues such as Leu487, Gly488, Glu489, Gly490, Cys491, Phe492, and Val495, that located over phosphate binding region of ATP (Fig. S1).

Considering non-covalent interactions between compound **A5** and homology model of FGFR3, hydrogen bonds were formed by amide group on the indolin-2-one ring with Asp518 and the positively charged tertiary amine group of *N*-methylpiperazine ring with Asp635 (Table S6, Fig. S2). Besides, compound **A5** formed direct hydrogen bonds with water molecules, and water bridges with backbone residues given in Table S8. In addition, an ionic bond formed by the positively charged tertiary amine group of *N*-methylpiperazine ring and the carboxylate group of Asp635 has provided the contribution to binding of compound **A5** into FGFR3 (Figs. S3–S4). Lastly, the phenyl ring of benzylidene group of compound **A5** has made contribution to form hydrophobic interactions with Phe483 and Arg655.

In terms of non-covalent interactions between compound **A13** and FGFR1, compound **A13** formed several hydrogen bonds with backbone residues given in Table S6. Besides, compound **A13** formed several hydrogen bonds with water molecules, and water-mediated hydrogen bonds with Ala564, Asn568 and Asp641 (Tables S7–S8, Fig. S5). The other non-covalent interaction determined between compound **A13** and FGFR1 is a salt bridge formed by the positively charged tertiary amine group of *N*-methylpiperazine ring and carboxylate group of Asp641 (Figs. S6–S7). It was also determined hydrophobic interactions between naphthalene ring of compound **A13** and amino acid residues of hydrophobic region I, and between indole-2-one ring and Leu484, respectively.

**3.4.2.3. MM-GBSA free binding energy calculations.** MM-GBSA free binding energies of compounds **A1**, **A5** and **A13** inside their target proteins were calculated from free MD simulations of compound **A1**-FGFR2, compound **A5**-FGFR3 and compound **A13**-FGFR1 complexes, and the estimated binding energies and their components were reported in Table S9. According to free binding energy calculations, van der Waals energy for compound **A1**-FGFR2 complex and electrostatic energy for compound **A5**-FGFR3 and compound **A13**-FGFR1 complexes are favorable energy component to contribute their estimated free binding energies. Van der Waals and non-polar solvation energy are main component of the estimated binding energy of compound **A1** inside FGFR2, which were supplied by Leu487, Gly488, Phe492, Val495, Lys517, Val564, and Ala567. These energies showed that hydrophobic and CH- $\pi$  interactions played an important role in the binding of compounds **A1** into FGFR2, besides hydrogen bonds (Table S6). For compound **A1**-FGFR2 complex, electrostatic energy (in vacuum and solvent), that was mostly provided by Glu534, made contribution to estimated free binding energy after van der Waals energy. Lys517,

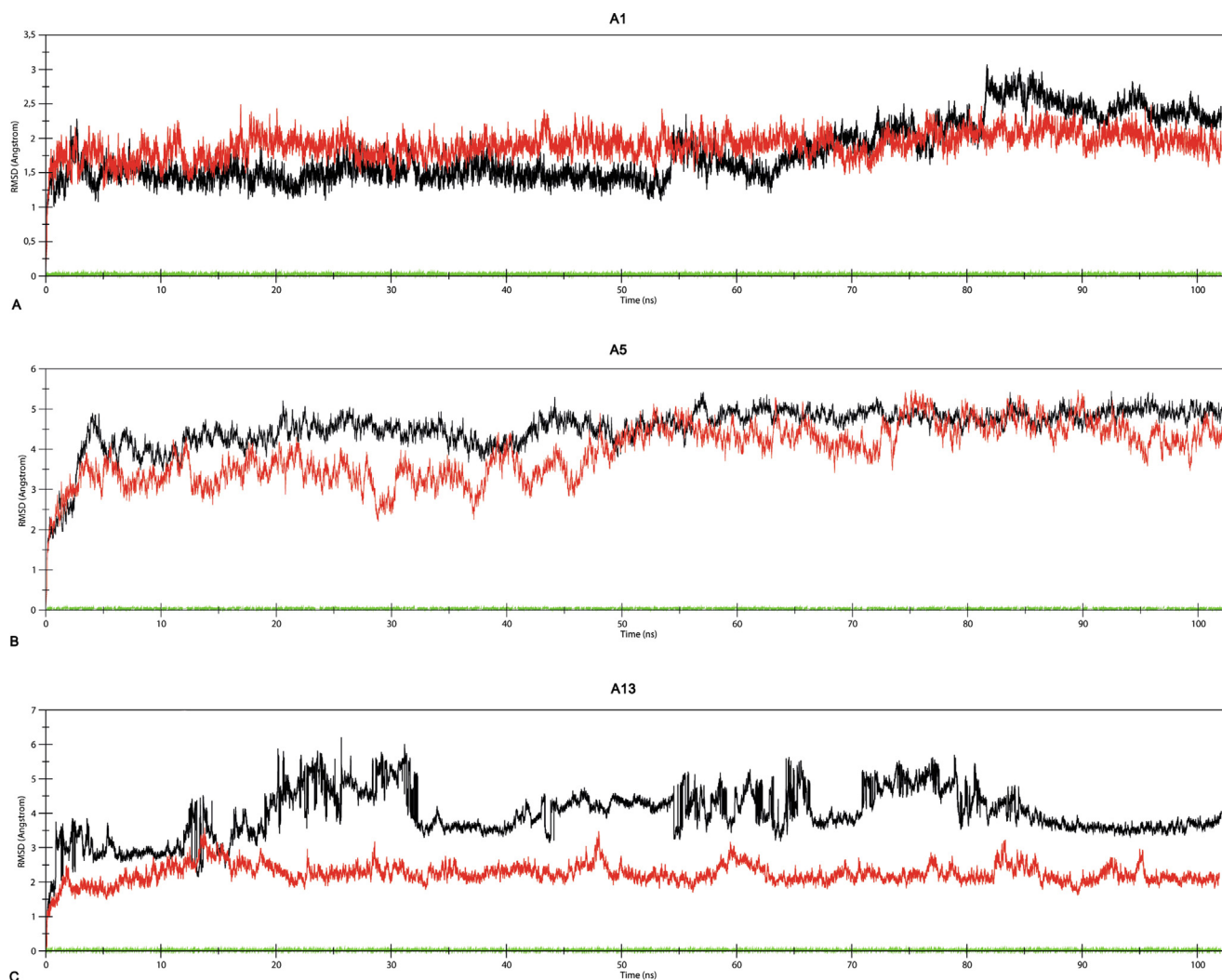


**Fig. 4.** (A) Plots of root-mean square deviation (RMSD) of FGFR2 and compound **A1**-FGFR2 complex. (B) Plots of root-mean square deviation (RMSD) of FGFR3 and compound **A5**-FGFR3 complex. (C) Plots of root-mean square deviation (RMSD) of FGFR1 and compound **A13**-FGFR1 complex. RMSDs were calculated using initial structures as templates. Green, red and black RMSD plots are represented for ligands, proteins and complexes, respectively. The trajectories were captured every 1 ps until the simulations end.

Ala567, Val495, and Phe492 are main contributors for electrostatic energy (in vacuum and in solvent) later than Glu534.

Electrostatic energy (in vacuum) is a major component for estimated free binding energy calculated from free MD simulations of compound **A5**-FGFR3 complex. According to energy composition analysis, amino acid residues such as Glu480, Gln485, Lys508, Asp518, Asp635, and Arg655 are main contributors for total electrostatic energy (in vacuum and in solvent). Especially, Asp518 made a major contribution for total electrostatic energy. Van der Waals and non-polar solvation energies are favorable energy components for ligand binding supporting the hydrophobic interactions formed by ligand and amino acid residues of FGFR3, have mostly supplied by amino acid residues such as Phe483 and Arg655, which are the main energy contributors for estimated binding energy of compound **A5**.

Regarding the estimated free binding energy of compound **A13**-FGFR1 complex, electrostatic energy (in vacuum) is a major component for the ligand binding. The main contributors for total electrostatic energy (in vacuum and in solvent) are amino acid residues such as Glu531 and Asp641. Besides, this energy also supports formation of salt bridge between compound **A13** and Asp641. Van der Waals and non-polar solvation energy are favorable energy compo-

ponents for estimated binding energy for compound **A13**, and provided by Leu484, Glu486, Val492, Lys514, Val561, Leu630, and Asp641. The calculated van der Waals and non-polar solvation energies have displayed the contribution of hydrophobic interactions for binding of ligand. The energy composition analysis results for compound **A1**, **A5** and **A13** were summarized in Tables S10, S11 and S12, respectively.

#### 4. Conclusions

In summary, we designed and synthesized 30 compounds based on SU4984, as an FGFR inhibitor, in order to evaluate biological activity potencies against FGFR1–4. All compounds displayed FGFR inhibition at the range of the studied concentrations. On the other hand, six compounds, bearing morpholine, 4-hydroxypiperidine and 4-methylpiperazine groups at C4' position, and 6-hydroxynaphthalene and 4'-hydroxy-(1,1'-biphenyl) groups at the C5 position displayed FGFR2 inhibition among the synthesized compounds. Besides, compounds **A1**, **A5** and **A13** have best inhibitory potencies against FGFR2, FGFR3 and FGFR1, respectively. And also, these compounds were found highly selective on the title FGFRs. According to molecular modelling studies, it was found



out compounds **A1** and **A13** occupied hydrophobic region I, adenine binding region of ATP and phosphate binding region of ATP inside FGFR2 and FGFR1, respectively. On the contrary, compounds **A5** occupied nucleotide binding domain of and phosphate binding region of ATP, and occupied elongating towards Arg655. Molecular dynamics confirmed to these binding orientations inside related proteins. Adding aromatic structures at the C5 position on indolin-2-on core progressed FGFR1 inhibitory potency in comparison to SU4984 ( $IC_{50} = 10\text{--}20\ \mu\text{M}$ , FGFR1). This gives opportunity to develop more potent and selective inhibitors against FGFR1. Besides, most of the compounds bearing *p*-amidophenyl groups at the C5 position of indolin-2-one displayed selective FGFR3 inhibition and this suggested that these derivatives could be lead compounds for the development of more effective and selective FGFR3 inhibitors.

### Declaration of Competing Interest

The authors confirm that this article content has no conflicts of interest.

### Acknowledgements

Authors would like to express their sincere thanks toward Turkish Scientific and Technical Research Council (TUBITAK) (Turkey, Grant number 115S692) and Ege University (Turkey, Grant number 2015/BİL/040), for their financial support, respectively. Authors appreciate to Pharmaceutical Sciences Research Centre (FABAL) of Ege University Faculty of Pharmacy for spectral analyses of the compounds and molecular modelling software support.

### Appendix A. Supplementary material

Supplementary data to this article can be found online at <https://doi.org/10.1016/j.sjps.2019.07.004>.

### References

- Ahmad, I., Iwata, T., Leung, H.Y., 2012. Mechanisms of FGFR-mediated carcinogenesis. *Biochim. Biophys. Acta* 1823, 850–860.
- Altman, M., Wilson, K., 2010. Inhibitors of janus kinases. *WO/2010/014453*.
- Beena, Kumar, D., Bailey, M.A., Parish, T., Rawat, D.S., 2014. Synthesis and antituberculosis activity evaluation of cyclohexane-1,2-diamine derivatives. *Chem. Biol. Interface* 4 (1), 23–36.
- Case, D.A., Darden, T.A., Cheatham, T.E., Simmerling, C.L., Wang, J., Duke, R.E., Luo, R., Walker, R.C., Zhang, W., Merz, K.M., Roberts, B., Hayik, S., Roitberg, A., Seabra, G., Swails, J., Goetz, A.W., Kolossváry, I., Wong, K.F., Paesani, F., Vanicek, J., Wolf, R. M., Liu, J., Wu, X., Brozell, S.R., Steinbrecher, T., Gohlke, H., Cai, Q., Ye, X., Wang, J., Hsieh, M. J., Cui, G., Roe, D.R., Mathews, D.H., Seetin, M.G., Salomon-Ferrer, R., Sagui, C., Babin, V., Luchko, T., Gusarov, S., Kovalenko, A., Kollman, P.A., 2012. Amber 12, University of California, San Francisco.
- Chen, G., Weng, Q., Fu, L., Wang, Z., Yu, P., Liu, Z., Li, X., Zhang, H., Liang, G., 2014. Synthesis and biological evaluation of novel oxindole-based RTK inhibitors as anti-cancer agents. *Bioorg. Med. Chem.* 22, 6953–6960.
- Essmann, U., Perera, L., Berkowitz, M.L., Darden, T., Lee, H., Pedersen, L.G., 1995. A smooth particle mesh Ewald method. *J. Chem. Phys.* 103, 8577–8593.
- Garcia-Maya, M., Anderson, A.A., Kendal, C.E., Kenny, A.V., Edwards-Ingram, L.C., Holladay, A., Saffell, J.L., 2006. Ligand concentration is a driver of divergent signaling and pleiotropic cellular responses to FGF. *J. Cell. Physiol.* 206, 386–393.
- Ghedini, G.C., Ronca, R., Presta, M., Giacomini, A., 2018. Future applications of FGF/FGFR inhibitors in cancer. *Expert Rev. Anticanc.* 18 (9), 861–872.
- Grace Development Team, <http://plasma-gate.weizmann.ac.il/Grace/>.
- Halgren, T.A., 1996. Merck molecular force field. I. basis, form, scope, parameterization, and performance of MMFF94\*. *J. Comput. Chem.* 17, 490–519.
- Heinzle, C., Sutterlüty, H., Grusch, M., Grasl-Kraupp, B., Berger, W., Marian, B., 2011. Targeting fibroblast-growth-factor-receptor-dependent signaling for cancer therapy. *Expert Opin. Ther. Tar.* 15 (7), 829–846.
- Hornak, V., Abel, R., Okur, A., Strockbine, B., Roitberg, A., Simmerling, C., 2006. Comparison of multiple Amber force fields and development of improved protein backbone parameters. *Proteins: Struct. Funct. Bioinf.* 65, 712–725.
- Jakalian, A., Bush, B.L., Jack, D.B., 2000. Fast, efficient generation of high-quality atomic charges. AM1-BCC model: I. method. *J. Comput. Chem.* 21, 132–146.
- Jia, Y., Quinn, C.M., Kwak, S., Talanian, R.V., 2008. Current *in vitro* kinase assay technologies: the quest for a universal format. *Curr. Drug Discov. Technol.* 5, 59–69.
- Jones, G., Willett, P., Glen, R.C., 1995. Molecular recognition of receptor sites using a genetic algorithm with a description of desolvation. *J. Mol. Biol.* 245 (1), 43–53.
- Jones, G., Willett, P., Glen, R.C., Leach, A.R., Taylor, R., 1997. Development and validation of a genetic algorithm for flexible docking. *J. Mol. Biol.* 267 (3), 727–748.
- Jorgensen, W.L., Chandrasekhar, J., Madura, J.D., 1983. Comparison of simple potential functions for simulating liquid water. *J. Chem. Phys.* 79, 926–935.
- Kas, S.M., de Ruiter, J.R., Schipper, K., Schut, E., Bombardelli, L., Wientjens, E., Drenth, A.P., de Korte-Grimmerink, R., Mahakena, S., Phillips, C., Smith, P.D., Klarenbeek, S., van de Wetering, K., Berns, A., Wessels, L.F.A., Jonkers, J., 2018. Transcriptomics and transposon mutagenesis identify multiple mechanisms of resistance to the FGFR inhibitor AZD4547. *J. Cancer Res.* 78 (19), 5668–5679.
- Kim, S.H., Ryu, H., Ock, C.-Y., Suh, K.J., Lee, J.Y., Kim, J.-W., Lee, J.-O., Kim, J.W., Kim, Y. J., Lee, K.-W., Bang, S.-M., Kim, J.H., Lee, J.S., Ahn, J.B., Kim, K.-J., Rha, S.Y., 2018. BGJ398, A pan-FGFR inhibitor, overcomes paclitaxel resistance in urothelial carcinoma with FGFR1 overexpression. *Int. J. Mol. Sci.* 19, 3164–3179.
- Li, C.J., Liu, J.-F., Li, W., Gibeau, A., Rogoff, H., 2014. Inhibitors of kinases and cancer stem cells, and methods of preparation and use thereof. *US 2014/0275033 A1*.
- Li, X., Guise, C.P., Taghipouran, R., Yosaatmadja, Y., Ashoorzadeh, A., Paik, W.K., Squire, C.J., Jiang, S., Luo, J., Xu, Y., Tu, Z.C., Lu, X., Ren, X., Patterson, A.V., Smail, J.B., Ding, K., 2017. 2-Oxo-3, 4-dihydroprimido[4, 5-d]pyrimidinyl derivatives as new irreversible pan fibroblast growth factor receptor (FGFR) inhibitors. *Eur. J. Med. Chem.* 135, 531–543.
- Liang, G., Chen, G., Wei, X., Zhao, Y., Li, X., 2013. Small molecule inhibition of fibroblast growth factor receptors in cancer. *Cytokine Growth F. R.* 24, 467–475.
- Miller III, B.R., McGee Jr., T.D., Swails, J.M., Homeyer, N., Gohlke, H., Roitberg, A.E., 2012. MMPBSA.py: an efficient program for end-state free energy calculations. *J. Chem. Theory Comput.* 8, 3314–3321.
- Mohammadi, M., McMahon, G., Sun, L., Tang, C., Hirth, P., Yeh, B.K., Hubbard, S.R., Schlessinger, J., 1997. Structures of the tyrosine kinase domain of fibroblast growth factor receptor in complex with inhibitors. *Science* 276, 955–960.
- Molecular Operating Environment (MOE 2016.08) Chemical Computing Group Incorporation, 1010 Sherbrooke Street West, Suite 910, Montreal H3A 2R7, Canada.
- Pettersen, E.F., Goddard, T.D., Huang, C.C., Couch, G.S., Greenblatt, D.M., Meng, E.C., Ferrin, T.E., 2004. UCSF Chimera – a visualization system for exploratory research and analysis. *J. Comput. Chem.* 13, 1605–1612.
- Porta, R., Borea, R., Coelho, A., Khan, S., Araujo, A., Reclusa, P., Franchina, T., Van Der Steen, N., Van Dam, P., Ferri, J., Sireira, R., Naing, A., Hong, D., Rolfo, C., 2017. FGFR a promising druggable target in cancer: molecular biology and new drugs. *Crit. Rev. Oncol. Hemat.* 113, 256–267.
- Roe, D.R., Cheatham III, T.E., 2013. PTRAJ and CPPTRAJ: software for processing and analysis of molecular dynamics trajectory data. *J. Chem. Theory Comput.* 9, 3084–3095.
- Ryckaert, J.P., Ciccotti, G., Berendsen, H.J.C., 1977. Numerical integration of the Cartesian equations of motion of a system with constraints: molecular dynamics of n-alkanes. *J. Comput. Phys.* 23, 327–341.
- Sun, L., Tran, N., Tang, F., App, H., Hirth, P., McMahon, G., Tang, C., 1998. Synthesis and biological evaluations of 3-substituted indolin-2-ones: a novel class of tyrosine kinase inhibitors that exhibit selectivity toward particular receptor tyrosin kinases. *J. Med. Chem.* 41, 2588–2603.
- Treu, M., Karner, T., Reiser, U., 2011. Compounds. *US 2011/0263565 A1*.
- Turner, N., Grose, R., 2010. Fibroblast growth factor signalling: from development to cancer. *Nat. Rev. Cancer* 10, 116–129.
- Wang, J., Wolf, R.M., Caldwell, J.W., Kollman, P.A., Case, D.A., 2004. Development and testing of a general amber force field. *J. Comput. Chem.* 25, 1157–1174.
- Wang, Y., Li, L., Fan, J., Dai, Y., Jiang, A., Geng, M., Ai, J., Duan, W., 2018. Discovery of potent irreversible pan-fibroblast growth factor receptor (FGFR) inhibitors. *J. Med. Chem.* 61 (20), 9085–9104.
- Webb, B., Sali, A., 2014. Comparative Protein Structure Modeling Using Modeller. *Current Protocols in Bioinformatics*. John Wiley & Sons Inc., Hoboken, New Jersey, US. 5.6.1-5.6.32.
- Wei, M., Peng, X., Xing, L., Dai, Y., Huang, R., Geng, M., Zhang, A., Ai, J., Song, Z., 2018. Design, synthesis and biological evaluation of a series of novel 2-benzamide-4-(6-oxy-N-methyl-1-naphthamide)-pyridine derivatives as potent fibroblast growth factor receptor (FGFR) inhibitors. *Eur. J. Med. Chem.* 154, 9–28.
- Zhu, W., Chen, H., Wang, Y., Wang, J., Peng, X., Chen, X., Gao, Y., Li, C., He, Y., Ai, J., Geng, M., Zheng, M., Liu, H., 2017. Design, synthesis, and pharmacological evaluation of novel multisubstituted pyridin-3-amine derivatives as multitargeted protein kinase inhibitors for the treatment of non-small cell lung cancer. *J. Med. Chem.* 60, 6018–6035.